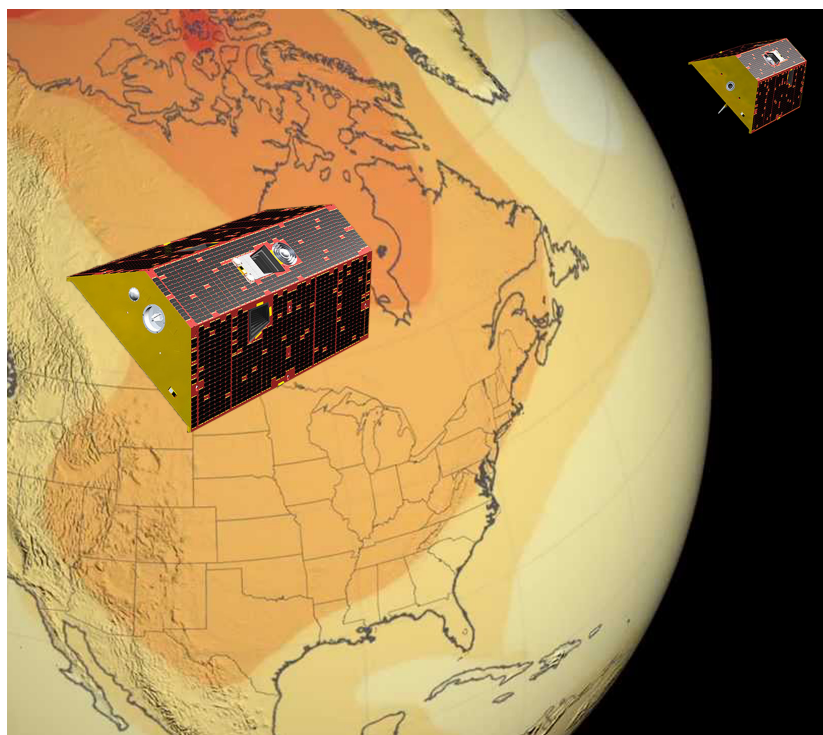


Characterizing storage-based drought using satellite gravimetry



Master Thesis

Peyman Saemian

Stuttgart, October 2021

Supervisors:

Prof. Dr.-Ing. Nico Sneeuw
University of Stuttgart

Dr.-Ing. Mohammad J. Tourian
University of Stuttgart

Erklärung der Urheberschaft

Ich erkläre hiermit an Eides statt, dass ich die vorliegende Arbeit ohne Hilfe Dritter und ohne Benutzung anderer als der angegebenen Hilfsmittel angefertigt habe; die aus fremden Quellen direkt oder indirekt übernommenen Gedanken sind als solche kenntlich gemacht. Die Arbeit wurde bisher in gleicher oder ähnlicher Form in keiner anderen Prüfungsbehörde vorgelegt und auch noch nicht veröffentlicht.

Ort, Datum

Unterschrift

Abstract

Drought is a complex phenomenon leading to a wide range of socio-economic, environmental, and political problems. The storage-based drought which represents the persistent lack of water in different levels of the Total Water Storage (TWS) from deep groundwater to surface water plays a vital role in proactive drought management. Despite its necessity, TWS could not be monitored due to the lack of consistent measurements from regional to continental scale. Since its launch in 2002, the Gravity Recovery and Climate Experiment (grace) mission and its successor GRACE Follow-On have provided unique observations of the TWS change at the global scale. In this study, we have investigated characterizing the storage-based drought at the global scale using GRACE measurements.

To this end, the Equivalent Water Height (EWH) has been retrieved from GRACE level 02 solutions. We have addressed the short record of GRACE observations in capturing the full hydro-climate variations. Based on our analysis, regions with a considerable direct human intervention like overexploitation of groundwater in the Middle East, regions that were affected by climate change like ice-melting over the Mackenzie river basin in Canada, or extreme precipitation events over the Ob river basin in the boreal regions are more sensitive to the length of ewh time series. Due to the crucial need for a long (at least 30 years) record of EWH, we have extended GRACE observations back to 1980 using an ensemble of models. The extended dataset has been developed using a pixel-wise selection of best-performed models among global hydrological models, land surface models, and atmospheric reanalysis models. The extended dataset has been used in the study for drought characterization over the grac period.

The proposed Storage-based Drought Index (SDI) successfully captured the documented drought events globally in terms of intensity and spatio-temporal distribution. Moreover, the analysis of SDI over the five classes of drought from D0 as abnormally dry to D4 as exceptional drought showed that most regions have suffered at least once from the storage-based drought over the GRACE period (2002–2016). Besides, the map of exceptional drought frequency highlights regions with significant groundwater extraction like California, the Middle East, and north of India and regions with exceptional shifts in the precipitation and temperature pattern and intensity like Amazon in South America and China. Finally, our comparison of SDI with three most widely used drought indices namely the Standardized Precipitation Index (SPI), the Standardized Precipitation Evapotranspiration Index (SPEI), and the Palmer Drought Severity Index (PDSI) reveals that despite their high correlation over climate-driven regions, these indices failed to characterize anthropogenic drought events, especially over regions with considerable groundwater withdraws. The study allows for a more informative storage-based drought with a more robust climatology as the reference, thus enabling a more realistic risk assessment.

Contents

1	Introduction	1
1.1	Introduction to drought	1
1.2	Storage-based drought	2
1.3	Problem Statement, Objectives and Outline	3
2	Drought monitoring	5
2.1	Drought versus aridity and heatwaves	7
2.2	Complexity of drought	9
2.3	Main drought indices	10
2.3.1	Standardized Precipitation Index	11
2.3.2	Palmer drought severity index	12
2.3.3	Standardized precipitation evapotranspiration index	14
2.4	U.S. drought monitoring	15
3	New storage-based drought index	17
3.1	Total Water Storage change from GRACE	17
3.2	Total water storage deficits	21
3.3	The short record of GRACE EWH	21
3.4	External climatology from models	22
3.5	The storage-based drought index (SDI)	25
4	Results and discussions	29
4.1	Global distribution of drought	29
4.2	Time evolution of drought for main catchments	29
4.3	Performance of the SDI during extreme hydrologic events	30
4.4	Comparison of SDI with other drought indices	32
4.5	Comparison of SDI with USDM	35
4.6	Comparison of different approach for calculating SDI	35
5	Summary and outlook	37
6	Appendixes	39
6.1	Satellite gravimetry applied to drought monitoring	39
6.2	Satellite gravimetry	40
6.3	GRACE satellite mission	41
6.4	Water storage change from GRACE	42

List of Figures

2.1	Sequence of drought occurrence and impacts for commonly accepted drought types (Wilhite, 2000)	6
2.2	Map of the global distribution of climatic zones (source: UNEP-WCMC)	8
2.3	Increase of the number of heatwaves during the last 3–4 decades. The number of deadly days have been selected globally during each year based on the average daily relative humidity and temperature (Mora et al., 2017).	9
2.4	Different drought indices for the continental United States (CONUS) June 2012.	15
3.1	Flowchart of obtaining EWH in this thesis.	18
3.2	The GRACE EWH for October 2006, before and after filtering (DDK3).	19
3.3	The GRACE EWH for April 2006, obtained from DDK1 to DDK8.	20
3.4	The GRACE EWH time series for the Tigris river basin in Iraq, obtained by applying DDK1 to DDK8 filters.	20
3.5	Time series of, Top:GRACE EWH, middle: climatology (obtained from the GRACE time period), and bottom: the GRACE EWH anomalies for the Tigris located in Iraq.	21
3.6	Long-term monthly mean (climatology) of EWH over selected basins within three periods namely 1980–2016 (40 years), 2002–2016 (GRACE observation period), and 1980–2002 (pre GRACE).	23
3.7	Linear trends obtained over the period 2002–2009 from the models.	24
3.8	EWH time series from GRACE observations and the ensemble of the models for selected basins.	25
3.9	The 4 main steps in calculating SDI from the original EWH time series. Here the results are shown for the Tigris basin in Middle East.	26
3.10	Left: The CDF distribution for the four best theoretical distribution functions (among 20 distribution functions) compared with empirical distribution. Tight: The related error in the three best best theoretical distribution compared with the empirical distribution	27
3.11	The projection of the percentile values for the different classes of drought on the empirical CDF of the long-time series of SDI for the Tigris basin. Quantile values will be then used for drought characterization	27
4.1	Global maps of drought characterization for July 2010, (a) gridded map and (b) basin-scale map.	29
4.2	Spatial distribution of the frequency for each class of drought within the GRACE period (2002–2016).	30
4.3	Time evolution of the SDI over selected basins.	31
4.4	SDI results during some reported droughts.	32
4.5	Comparison of drought indices namely SPI, SPEI, and PDSI with SDI over selected basins. The basins are located in regions with considerable groundwater extraction.	33

4.6	Comparison of drought indices namely SPI, SPEI, and PDSI with SDI over selected basins.	34
4.7	Trends in EWH (in centimetres per year) based on GRACE observations from April 2002 to March 2016 together with the possible interpretation over certain spots (Source: (Rodell et al., 2018)).	34
4.8	Drought classification from USDM, SDI, and SDI using only GRACE for the CONUS during August 2011 and February 2016.	35
4.9	The storage-based drought index under different scenarios over selected basins: column (a) shows all together, column (b) illustrates the approach proposed in this study (SDI), column (c) depict the SDI but using GRACE climatology, and colume (d) shows the SDI but over a detrended EWH.	36
6.1	The static (average) Earth's gravity field (EGM08 model, from Pavlis et al. (2008)). Source: Bureau Gravimetrique International.	40
6.2	Concepts of: a: satellite-to-satellite tracking in the high-low mode (SST-hl); b: satellite-to-satellite tracking in the low-low mode (SST-ll) combined with SST-hl; c: satellite gradiometry combined with SST-hl	41
6.3	GRACE is a twin satellite mission orbiting the Earth at an initial altitude of about 500 km in a polar orbit (89°inclination), and 220 km apart (source: NASA).	42

List of Tables

2.1	Phenomena reflected by specific-duration standardized precipitation indices (SPI) and their applications (NDMC)	12
2.2	drought/wetness classification by SPI	12
3.1	Summary of datasets used in this study.	24
3.2	USDM classification for drought characterization (Svoboda et al., 2002)	26

Chapter 1

Introduction

1.1 Introduction to drought

Water plays a vital role in all sectors of our society including agricultural, industrial, and energy sectors. Earth is known as a blue planet. There is no shortage of water as nearly 70 percent of our planet is covered by water (about 326 million trillion gallons of water). Water can freeze into ice or evaporate into the air, but it does not leave our planet. Despite its abundance, only 2.5 percentage of all those water is freshwater and the rest is saltwater. Even then, we only access just 1 percent of our freshwater while much of it is trapped in glaciers and snowfields. Essentially, only 0.007 percent of the Earth's water is available to fulfill human needs and access to it depends on where we live.

Water scarcity occurs almost every year in many parts of the world. On one hand, the demand for water for each of these sectors has increased manyfold due to the growth of population (UN, 2012). On the other hand, the amount of sources for fulfilling this water demand is limited. Other factors, such as climate change and contamination of water supplies, aggravate this unequal supply-demand balance. It is expected that over the coming decades, we will live in a warmer world with more climatic extremes, including drought which will bring socio-political tensions.

Drought is a recurring hazard with slow onset. It can be the consequence of anthropogenic effects, natural change in the climate, or the combination of these two. Drought produces a complex web of impacts that accumulate over a considerable period of time (e.g., weeks to months). It can virtually affect any climate region and has wide-ranging impacts on many sectors of society. Drought ranks among the most costly of the all-natural disaster (Bruce, 1994; Obasi, 1994). Half of the world's terrestrial surface is prone to drought. As a result, drought is a widespread phenomenon (Kogan, 1997).

To reduce the damage from them, it is crucial to characterize droughts. This enables operations such as drought early warning (Kogan, 2000) and drought risk analysis (Hayes et al., 2004). Among several methodologies, quantitative measures called drought indices are prevailing for drought characterization (Tsakiris et al., 2007). These indices characterize drought levels by incorporating data from one or several variables (indicators) such as precipitation and evapotranspiration into a single numerical value (Zargar et al., 2011).

Scientists have developed such indices using multiple factors including drought nature and characteristics and the impacts considered. Manifold drought indices have been developed (more than 150, [Niemeyer et al. \(2008\)](#)). The nature of drought indices reflects different events and conditions; they can reflect climate dryness anomalies (mainly based on precipitation) or correspond to delayed agricultural and hydrological impacts such as soil moisture loss or lowered reservoir levels. In addition, the categorization of drought indices can also be based on the data and technology used. For example, a considerable number of indices use remote-sensing imaging to detect vegetation health as an indicator of drought.

1.2 Storage-based drought

The terrestrial water storage (TWS) is defined as the total water stored on the surface (e.g., lakes, reservoirs, rivers, and snow water equivalent), over the entire soil profile, and in groundwater. TWS is a key part of the global hydrological cycle and plays a major role in Earth's climate system exerting important control over the water, energy, and biochemical fluxes ([Famiglietti, 2004](#)). It shows the variation in the combination of all mentioned components and is blind to their separate change. However, it has the potential to consider a deficiency in some of those elements (e.g., groundwater) that are hard to track individually.

In spite of its importance, until recently TWS has not been adequately measured at the continental scale ([Lettenmaier and Famiglietti, 2006](#)). Traditional monitoring of terrestrial water storage mainly depends on in situ measurements and model simulations. On one hand in situ data, including boreholes, soil moisture stations, and lake water level measurements are too costly to have an adequate network of measuring stations. Furthermore, statistical interpolation methods will bring an additional error into spatially continuous data. On the other hand, land surface models (LSMs) or hydrological models are able to simulate components of TWS. However, these models often lack important components of TWS in their process, e.g., groundwater or deep soil moisture ([Rodell et al., 2004b](#)). It is difficult to evaluate the reliability of TWS and its component from LSMs due to the lack of in situ data ([Long et al., 2015](#)).

From 2002 to 2017, the GRACE (Gravity Recovery and Climate Experiment) mission provided a precise survey of Earth's time-variable gravity field, with unprecedented temporal (monthly) and spatial (down to the scales of a few hundred kilometers) sampling ([Tapley et al., 2004](#)) (see Appendix A for more details). GRACE has measured and monitored monthly changes in how mass is redistributed within and among Earth's atmosphere, oceans, land, and ice sheets, as well as within Earth itself. The mission followed by the Gravity Recovery and Climate Experiment Follow-On (GRACE-FO) mission, was launched on May 22, 2018. The GRACE-FO will continue its predecessor mission by providing the Earth's time-variable gravity field, testing new technology. From the hydrologic perspective, the main product of GRACE mission is the Terrestrial Water Storage change (ΔTWS): monthly change in the total water stored on the surface (e.g., lakes, reservoirs, rivers, and snow water equivalent), over the entire soil profile, and in groundwater.

During the last decade, GRACE-based observations of Δ TWS have been used extensively to quantify and understand hydrological processes encompassing evapotranspiration estimation (e.g., Rodell et al. (2004a); Long et al. (2014); Castle et al. (2016)), snow water equivalent volumes (Frappart et al., 2006), groundwater storage change (e.g., Rodell et al. (2009); Sun et al. (2012); Chen et al. (2016); Scanlon et al. (2015)), and river basin discharge (Syed et al., 2005). The contribution of GRACE in assessing large-scale hydrological extremes, namely drought and flood, started as the temporal length of GRACE increased. In particular, storage-based and groundwater droughts have been introduced into the drought monitoring community using GRACE-based estimates of Δ TWS. Although GRACE is blind to individual components, it has the potential to detect a deficiency in some of those elements (e.g., groundwater). As a result, a GRACE-based drought indicator provides more holistic and realistic diagnoses of drought conditions than commonly used indices like the standardized precipitation index (SPI) and Palmer drought severity index (PDSI)), at regional scales (Houborg et al., 2012; Long et al., 2013).

During the last decade, several studies have investigated the contribution of GRACE-based storage change products to drought monitoring. The early contribution of GRACE with drought identification evoked by Seitz et al. (2008). Then, Yirdaw et al. (2008) employed GRACE to identify the 2002/2003 Canadian Prairie droughts and introduced the total storage deficit index (TSDI). Afterward, Chen et al. (2010) utilized TWS anomaly from GRACE to identify drought events in the La Plata basin, in Argentina. Houborg et al. (2012) developed GRACE-based drought indicators and enhanced its spatial resolution using data assimilation. Long et al. (2013) and Wang et al. (2014) investigated the correlation between the depletion in GRACE TWSA time series and the drought events in Texas and the Haihe river basin (HRB) in Northern China, respectively. Recently some more sophisticated drought indices using GRACE TWS anomaly have been introduced (e.g., GRACE-based Hydrological Drought Index (GHDI) by Yi and Wen (2016), and GRACE-DSI by Zhao et al. (2017a)).

1.3 Problem Statement, Objectives and Outline

Problem Statement GRACE satellite mission has provided unique information much-needed for the global tracking of water storage changes until late 2017. Moreover, its successor, the GRACE follow-on mission, was launched in early 2018. Existing GRACE-based drought indices in some basins showed high correlation with other drought indices and have been suggested as a tool for drought monitoring and risk management. However, most of those indices suffer from the relatively short length of the GRACE time series. GRACE-based indices have correctly identified several historical drought events. However, the classification of storage-based droughts has remained incomplete as several events have been characterized with a different class of severity and in some cases duration.

Objectives The overall objectives of this study are:

- 1 to establish a new storage-based drought index
- 2 to characterize storage-based drought events globally using the new index

- 3 to determine the performance of the new drought index in identifying some globally well-known drought events during the time period of GRACE
- 4 to compare the GRACE-based dimensionless drought index with common drought indices such as the Standardized Precipitation Index (SPI), the Palmer Drought Severity Index (PDSI), and the Standardized Precipitation Evapotranspiration Index (SPEI).

During establishing the new index, we investigate the steps proposed in the literature. For example, we examine the effect of detrending the GRACE EWH time series for drought characterizing. We also evaluate the short data record length of GRACE EWH to sample the full range of wetness and dryness required.

Outline In chapter 2, the main concepts related to drought monitoring in general and the contribution of GRACE in drought monitoring will be discussed. The main part of the methodology, including handling GRACE products and challenges to achieve a GRACE-based drought index, is explained in chapter 3. Moreover, in this chapter, possible solutions to each of those challenges will be elaborated. The result of the drought index (both spatial and temporal evolution) is presented in chapter 4. Furthermore, the GRACE-based drought index is compared with the main historical drought events around the world and with other drought indices in this chapter. Finally, the summary and outlook are provided in Chapter 5.

Chapter 2

Drought monitoring

Drought is a complex phenomenon with not a specific single universally accepted definition. Therefore, it is difficult to identify its key characteristics such as duration, severity, and spatial extent. However, drought can be traditionally classified according to three physically-based perspectives ([Mishra and Singh, 2010](#)):

- Meteorological: lack of precipitation
- Agricultural : deficit in soil moisture and vegetation response
- Hydrological: deficit in the runoff, streamflow, or groundwater storage

Moreover, a new class of drought called socio-economic drought ([Mehran et al., 2015](#)), also termed as anthropogenic drought ([AghaKouchak, 2015](#)), has been proposed recently. It is mainly related to the overuse or abuse of water due to human activities that can lead to water stress in an area.

The four perspectives of drought are different in timing, impact, and recovery rate with a rapid sense of dryness in meteorological drought, an intermediate response in agricultural and long-term dryness indicative of hydrological drought ([Figure 2.1](#)). It can be concluded from the figure that drought designations among sectors may or may not coincide in space and time ([Wilhite, 2000](#)). This means that several weeks of dryness may trigger an agricultural drought but it may not be sensed by groundwater or have little effect on streamflow. Moreover, the same duration of dryness may cause a severe drought in one region but may be classified as just abnormally dry in one another.

Drought, either due to natural effects or due to human activities, requires taking measures to counteract it. Traditionally, our responses to drought events have been conducted in a very reactive, post-event fashioned which has been called *crisis management*. A crisis is an event that occurs at a specific time that is usually unforeseen, public in nature, and has the potential to cause great harm to different sectors. In contrast, a risk is an activity or event that has the potential to harm those sectors. Whereas crisis management is concerned with responding to, managing, and recovering from an unforeseen event, *risk management* is concerned with identifying, assessing, and mitigating activities or events that could harm society. Risk management in the drought concept includes preparedness planning, mitigation, monitoring, and early warning, and also prediction to reduce the impacts of drought. Drought monitoring, defined as tracking the severity and location of drought, plays a vital role in this risk-based

management frame. It can be considered as a pillar source for a successful drought policy besides the impact assessment and mitigating.

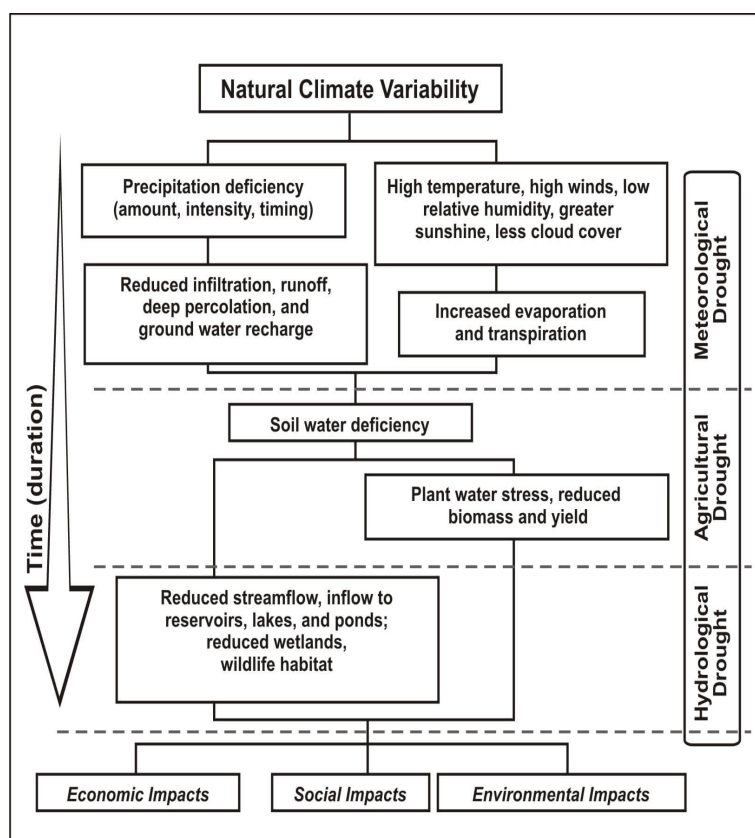


Figure 2.1: Sequence of drought occurrence and impacts for commonly accepted drought types (Wilhite, 2000)

Droughts can occur due to shortage and reduction of water in any compartment of the water resources, e.g., lakes, surface water resources, or underground water. Also, during the past 50 years, many efforts have emphasized climate- and hydrological-based indicators and indices that track fluctuations in the components of the hydrological cycle (e.g., precipitation, temperature, streamflow, and soil moisture). As a result, one of the main goals in drought monitoring development is to improve the ability to provide relevant and timely drought information. This information can be delivered to decision-makers as an early warning.

The more we know about drought and its definitions, the better we can investigate and monitor it. As a result, in this chapter, we will discuss the complexity of drought and drought monitoring. Definitions, characteristics of drought, and the challenges it presents for effective monitoring and early warning for risk management goals are explained. Aridity and heat waves are not categorized in drought. Differences between these two phenomena with drought are elaborated further in this chapter. Finally, the role of spaceborne sensors augmenting the in situ-based climate and hydrology data for the use of drought monitoring for both *past* and *present* are introduced.

2.1 Drought versus aridity and heatwaves

Three terms namely drought, aridity, and heatwaves have different definitions that need to be discussed before further steps in understanding drought. Aridity is defined, in meteorology and climatology, as the degree to which a climate lacks effective, life-promoting moisture (Glossary of Meteorology, American Meteorological Society). In other words, aridity is a permanent feature of climate which is restricted to low rainfall areas (Wilhite, 1992). It is widespread in the drylands of the world, where a shortage of water prevails through the whole, or most of, the year. While in contrast, drought is a temporary aberration and can occur in virtually all climate zones, both in high and low rainfall areas (Mishra and Singh, 2010).

Aridity is measured by comparing long-term average water supply (precipitation) to long-term average water demand (evapotranspiration). If demand is greater than supply, on average, then the climate is arid. Aridity can be investigated mainly based on (1) climate variables (index of aridity), or (2) the number of days when water balance favors plant growth (length of the growing season) (Kassas, 2008). Drought, on the other hand, is defined as a period of abnormally dry weather, sufficiently long enough to cause a serious hydrological imbalance.

The Food and Agriculture Organization of the United Nations (FAO), has used freely available satellite images and found that 41 percent of the world's land surface—an area twice the size of Africa— can be classified as drylands. Drylands are divided into four aridity zones. The least arid of the four is the dry sub-humid zone, such as the Sudanian savanna in West Africa, the grasslands in South America, the steppes in southern Siberia, and the Canadian prairie. Most dryland forests occur in this zone, as do some large irrigated, intensively farmed areas along perennial rivers. The driest is the hyper-arid zone, which is dominated by deserts, including the Sahara and the Arabian desert (Figure 2.2).

As the temperature (surface and air) is rising and the precipitation patterns are shifting during recent decades, the frequency of both droughts and heatwaves are increasing. However, drought and heatwave represent each a different phenomenon (Chang and Wallace, 1987). Whilst there is no conclusive definition for each of these two related events, we can define them as follow: Heatwave clearly comprises exceptionally high air temperatures that last for several days (can continue to even several weeks). The descriptive phrase of *high air temperature* can vary in a different part of the world, related to their climate. For example in the USA, a heatwave is defined as a period of more than three consecutive days where temperatures exceed 32.2°C (90°F), while in central Europe, the term heatwave normally refers to periods of several days when the maximum daytime air temperatures exceed 30°C. On the other hand, drought is commonly understood to be a relative concept that denotes reduced water availability in a particular region for a period that exceeds the long-term average. The combination of a heatwave and drought has dire socio-economic consequences (Mishra and Singh, 2010). It is worthwhile to mention that extreme heat events are responsible for more deaths annually than hurricanes, lightning, tornadoes, floods, and earthquakes combined (Min et al., 2011).

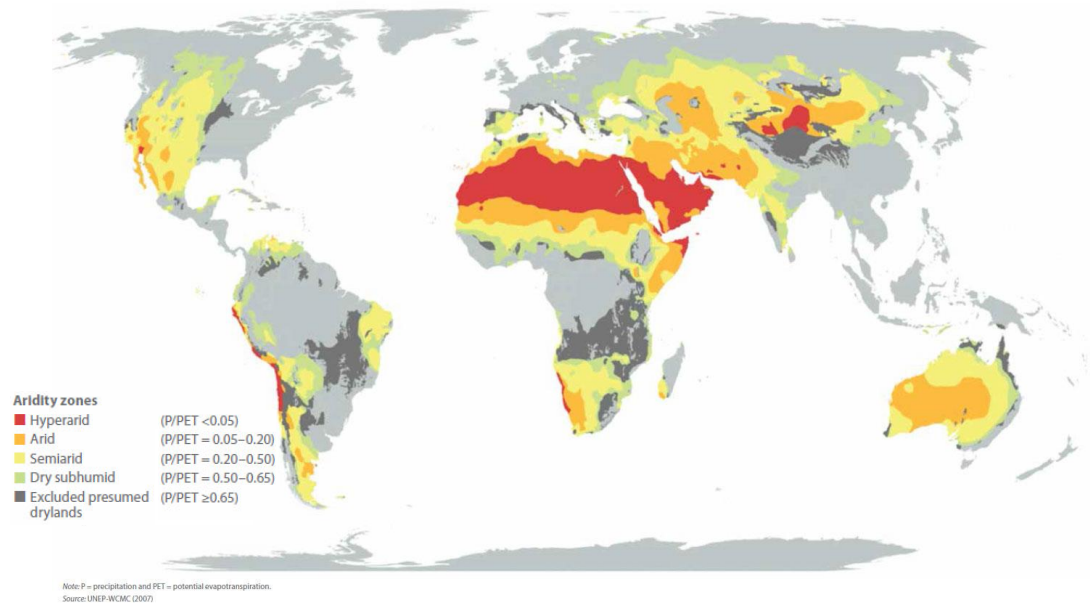


Figure 2.2: Map of the global distribution of climatic zones (source: UNEP-WCMC)

Numerous studies have documented that human-induced climate change has increased the frequency and severity of heatwaves across the globe (Jones et al., 2007; Gutowski et al., 2008; Hansen et al., 2012; Meehl et al., 2009). The combination of high humidity and high night-time temperature (known as high-humidity heatwaves) can make for a deadly pairing (referred to as hyperthermia), offering no relief and posing a particular threat for the elderly. It has shown an increasing trend during past 3–4 decades (Coumou and Rahmstorf, 2012; Russo et al., 2015; Mora et al., 2017) (see Figure 2.3). Droughts and heatwaves are connected (persistent heatwaves may lead to a class of drought). As an example, the prolonged drought over large parts of Europe is associated with the summer heatwave in 2003.

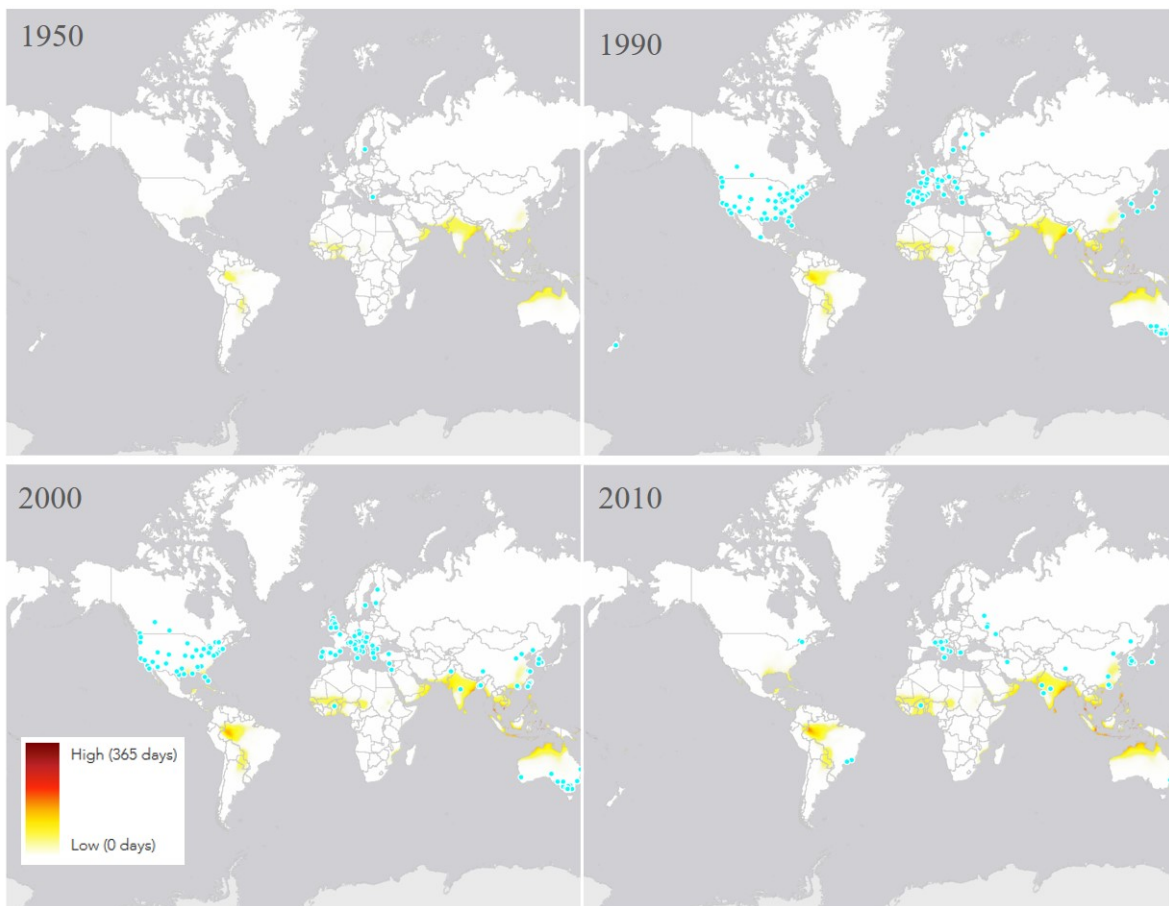


Figure 2.3: Increase of the number of heatwaves during the last 3–4 decades. The number of deadly days have been selected globally during each year based on the average daily relative humidity and temperature (Mora et al., 2017).

2.2 Complexity of drought

According to Wilhite (2000), drought is one of the most complex, but least understood among all natural hazards (e.g., floods, earthquakes, hurricanes). Even though this was mentioned in Wilhite’s book about 18 years ago, it is still true for some reasons. First, a worldwide accepted definition of drought is still missing. Although numerous definitions have been proposed so far, the literature lacks one precise definition that fulfills both the scientific and policymaker’s expectations. The difficulty of defining drought comes from the different points of view of several sectors. Consequently, the thresholds for declaring drought are arbitrary in most cases. Moreover, drought is defined as a natural phenomenon while in many cases, distinguishing between the role of nature and humans would be quite difficult. The recent human activities adversely affected the climate and water resources. These anthropogenic actions have led to accelerating, intensifying, and even in some cases triggering some severe droughts worldwide. Application and region-related definitions of drought seem more realistic and pragmatic, even for the decision-makers.

Second, drought is known as a creeping phenomenon. It may stay in a region for years after the termination, which makes the determination of the onset and the end of drought quite challenging. Drought is characterized by determining its onset, termination, and intensity.

Third, in contrast to floods, hurricanes, earthquakes, and tornadoes the effects of drought are non-structural and seldom result in structural damage (Mishra and Singh, 2010). Moreover, drought affects a wide geographical area, in most cases wider than any other natural hazard. Because of these two features, quantifying the impact and damages is quite a burdensome task compared with other natural hazards.

Drought indices summarise the complexity of drought into a single number and have improved drought monitoring and mitigation. In the following, some of the most widely used drought indices among the extensive list of them are explained.

2.3 Main drought indices

Several drought indices have been developed so far, each related to one or two different classes of drought (i.e., meteorological, agricultural, hydrological, and socio-economical droughts). Zargar et al. (2011) reviewed 74 operational and proposed drought indices and describes research directions. In each of these indices either the deficiency in water for each component of the TWS or the impact of drought (i.e., change in the vegetation quality and quantity) have been considered to develop the index. Some of the more common and practical indices include:

- Palmer Drought Severity Index (PDSI; Palmer (1965))
- Rainfall Anomaly Index (RAI; Van Rooy (1965))
- Crop Moisture Index (CMI; Palmer (1968))
- Bhalme and Mooly Drought Index (BMDI; Bhalme and Mooley (1980))
- Surface Water Supply Index (SWSI; Shafer (1982))
- Standardized Precipitation Index (SPI; McKee et al. (1993); McKee (1995))
- Vegetation Condition Index (VCI; Liu and Kogan (1996))
- Soil Moisture Drought Index (SMDI; Hollinger et al. (1993))
- Standardized Precipitation Evapotranspiration Index (SPEI; Vicente-Serrano et al. (2010))

Each of the indices has its own strengths and weaknesses. In what follows, some of the most widely used indices are introduced briefly. These indices will be to be compared further with the proposed GRACE-based drought index.

2.3.1 Standardized Precipitation Index

Description McKee et al. (1993) introduced the Standardized Precipitation Index (SPI) as a simple, easy to calculate, and statistically relevant drought index. It measures accumulated precipitation deficits over varying timescales from sub-seasonal to interannual. SPI can be computed for a variety of timescales. It represents the surface soil moisture (SM) variability in shorter timescales, the streamflow and reservoir levels in medium scales, and groundwater variations for longer timescales (Mishra and Singh, 2010). SPI is originally calculated for 3-, 6-, 12-, 24- and 48-month timescales. Table 2.1 shows the phenomena reflected and the application by each of these timescales up to 12-months timescales. These timescales represent the impact of drought on the availability of the different water resources. However, SPI only quantifies the precipitation deficit. Hence, it is highly sensitive to the preliminary data and the length of the record.

Calculation The SPI is calculated in the following sequence:

- Preparing a monthly precipitation data set for a period of m months, ideally a continuous period of at least 30 years. We refer to that as the long-term time series.
- For a i -month timescale, accumulate the precipitation values from month $j - (i - 1)$ to month j and attribute to month j .
- Fitting the Gamma probability distribution to the long-term accumulated precipitation.
- Calculating the probability of observed precipitation using Cumulative Distribution Function (CDF) from the fitted distribution.
- Finally, transferring the calculated probability to the standard normal variate (Z-score) using inverse standard normal CDF. Z-score for precipitation data is termed as SPI.

Typically, precipitation has a negatively skewed distribution i.e. smaller magnitudes occur with larger frequencies. Thus, instead of a common normal Probability Distribution Function (PDF), Gamma distribution provides a better fit for the data. The probability density function of the gamma distribution is defined as:

$$g(x) = \frac{1}{\beta^\alpha \Gamma(\alpha)} x^{\alpha-1} e^{-x/\beta} \quad \text{for } x > 0, \quad (2.1)$$

where $\alpha > 0$ is a shape parameter, $\beta > 0$ is a scale parameter, $x > 0$ is the amount of precipitation, and $\Gamma(\alpha)$ is the gamma function. More detailed descriptions of the gamma distribution can be found in Lloyd-Hughes and Saunders (2002) and Guttman (1998).

Table 2.1: Phenomena reflected by specific-duration standardized precipitation indices (SPI) and their applications (NDMC)

SPI duration	Phenomena reflected	Application
1 [mo]	Short-term conditions	Short-term soil moisture and crop stress (especially during the growing season)
3 [mo]	Short- and medium-term moisture conditions	A seasonal estimation of precipitation
6 [mo]	Medium-term trends in precipitation	Potential for effectively showing the pre- -precipitation over distinct seasons. e.g., for California, the 6 month SPI can effectively indicate of the amount of pre- -precipitation from Oct. to Mar.
9 [mo]	Precipitation patterns over a medium time scale	If $SPI_9 < -1.5$ then it is a good indication that substantial impacts can occur in agriculture (and possibly other sectors)
12 [mo]	Long-term precipitation patterns	Possibly tied to streamflows, reservoir levels, and also groundwater level

Table 2.2: drought/wetness classification by SPI

SPI value	drought/wetness condition
2.00 or more	Extremely wet
1.50–1.99	Severely wet
1.00–1.49	Moderately wet
0.00–0.99	Mildly wet
-0.99–0.00	Mild drought
-1.49–1.00	Moderate drought
-1.99–1.50	Severe drought
-2 or less	Extreme drought

2.3.2 Palmer drought severity index

Description The Palmer Drought Severity Index (PDSI) is perhaps the most widely used regional drought index for monitoring drought. [Palmer \(1965\)](#) formulated PDSI by estimating moisture supply and demand using precipitation and temperature as the inputs of a two-layer soil model. Despite its widespread application, PDSI inherit some limitations including:

- PDSI assumes all precipitation as rainfall (i.e., no contribution for snowfall) which makes the use of it problematic in winter and at high elevations.
- It responses slowly to developing and diminishing droughts ([Hayes et al., 1999](#)).

- PDSI is more applicable for agricultural droughts due to its innate time scale (Alley, 1984; Guttman, 1998; McKee, 1995; Willeke et al., 1994).

Calculation Here we explain the methodology for calculating PDSI mainly based on the Palmers paper (Palmer, 1965). The paper describes in detail how to calculate the PDSI using a 1-month time step. First, for each month of every year, four values related to the soil moisture and their complementary potential values are computed. These eight values are evapotranspiration (ET), recharge (R), runoff (RO), loss (L), potential evapotranspiration (ET_p), potential recharge (PR), potential runoff (PRO), and potential loss (PL). The four potential values are weighted according to the climate of the area using α , β , γ , and δ . These weighted factors are called the water balance coefficients and are calculated using the following equation:

$$\alpha_i = \frac{\overline{ET_i}}{\overline{ET_{p,i}}}, \quad \beta_i = \frac{\overline{R_i}}{\overline{PR_i}}, \quad \gamma_i = \frac{\overline{RO_i}}{\overline{PRO_i}}, \quad \delta_i = \frac{\overline{L_i}}{\overline{PL_i}} \quad (2.2)$$

where i ranges over the months of the year. The bar over a term indicates an average value for the whole time period of data. The weighted factors give us the climatically appropriate for existing conditions CAFEC potential values. The CAFEC precipitation, \hat{P} , is calculated using a combination of potential values. It represents the amount of precipitation needed to maintain a normal soil moisture level for a single month:

$$\hat{P} = \alpha_i ET_p + \beta_i PR + \gamma_i PRO - \delta_i PL \quad (2.3)$$

The difference between actual precipitation and \hat{P} is called the moisture departure denoted d :

$$d = P - \hat{P} \quad (2.4)$$

The interpretation of d is both time and spatial-dependent. This prevents straightforward comparisons from being made between different values of d . To overcome that, the moisture departure is weighted using K , which is called the climatic characteristic. To calculate K , Palmer derived two following equations:

$$K'_i = 1.5 \log_1 0 \left(\frac{\overline{ET_{p,i}} + \overline{R_i} + \overline{RO_i}}{\overline{P_i} + \overline{L_i}} \frac{1}{\overline{D_i}} + 2.8 \right) + 0.5 \quad (2.5)$$

$$K_i = \frac{17.67}{\sum_{j=1}^{12} \overline{D_j} K'_j} K'_i \quad (2.6)$$

The value 17.67 is an empirical constant that Palmer derived using data from nine locations in seven states of the United States (Palmer, 1965). The result of multiplying the moisture departure, d , by K is called the moisture anomaly index, or the Z index, shown as:

$$Z = dk \quad (2.7)$$

The Z index is used to calculate the PDSI value for a given month using the following formula:

$$X_i = 0.897X_{i-1} + \left(\frac{1}{3}\right)Z_i. \quad (2.8)$$

The two constant values in the formula, called the duration factors, were derived empirically by Palmer from two stations, western Kansas and central Iowa, and affect the sensitivity of the index to the precipitation events.

2.3.3 Standardized precipitation evapotranspiration index

Description The Standardized Precipitation Evapotranspiration Index (SPEI) first introduced by [Vicente-Serrano et al. \(2010\)](#) has been applied in comparative studies. SPEI measures the combination of water supply (precipitation) and water demand (evapotranspiration as computed from temperature). Warmer temperatures tend to increase evapotranspiration, which generally makes droughts more intense. The SPEI extends the SPI by incorporating precipitation and evapotranspiration in determining drought and shows advantages over the SPI in capturing temperature impact on water demand. Unlike PDSI, which closely tracks soil moisture levels within the upper soil layer, SPEI like SPI is more sensitive to the main component of the terrestrial water balance ([Guttman, 1998](#)). It has been claimed that SPEI outperforms the two aforementioned indices (SPI and PDSI) by taking their weaknesses into account.

Calculation SPEI is calculated in a similar method as SPI, but instead of only precipitation, we use the climatic water balance. The climatic water balance is defined as the difference between precipitation and potential evapotranspiration. Drought results from an imbalance between these two components. Water demand is usually measured by evapotranspiration (the amount of water that would be evaporated and transpired by plants). There is a distinction made between potential evapotranspiration (ET_p) and actual evapotranspiration (ET_a). ET_p is the demand or maximum amount of water that would be evaporated if enough water were available (from precipitation and soil moisture). ET_a is how much water, in reality, is evaporated and is limited by the amount of water that is available. ET_a is always less than or equal to ET_p , so ET_p is used for the water demand component of the drought equation.

The spatial distribution of the aforementioned drought indices namely SPI, PDSI, and SPEI is shown in [Figure 2.4](#) over the continental United States (CONUS) for June 2012. SPI and SPEI share the same pattern and intensity while PDSI shows drought over a larger extent and with higher intensity. The difference in the PDSI can be explained as it is also sensitive to the variation of the soil moisture which is not explored for the other two indices.

The drought maps provided weekly by the U. S. Drought Monitor (USDM) are one of the most widely used quantitative information in many studies for validation and comparison. To produce these maps, USDM uses many indices and indicators, which makes the final results more robust. In the thesis, we have compared our results with USDM maps for certain events. [section 2.4](#) provides introduce USDM briefly.

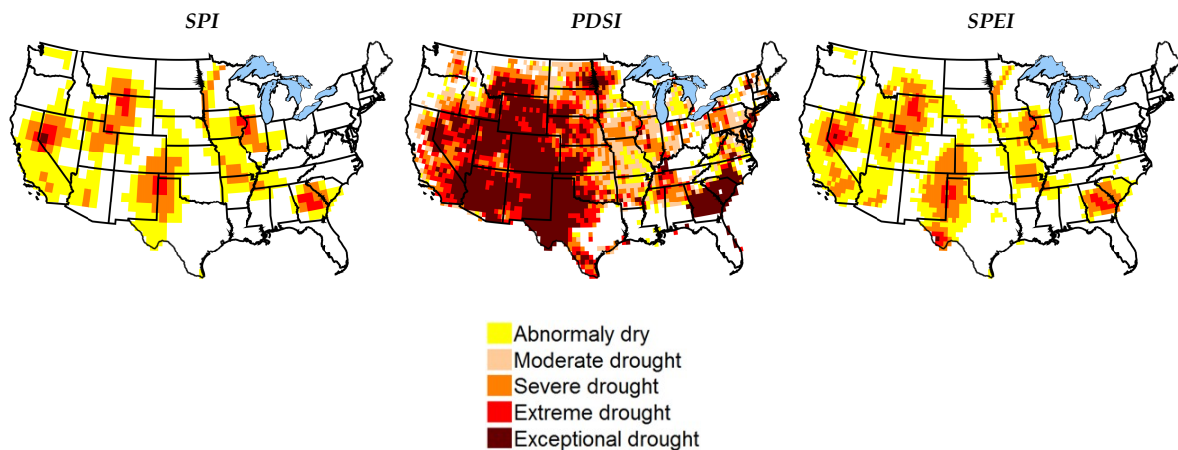


Figure 2.4: Different drought indices for the continental United States (CONUS) June 2012.

2.4 U.S. drought monitoring

The U.S. Drought Monitor (USDM), established in 1999, releases a weekly map of drought conditions in the United States. These maps are produced jointly by the National Oceanic and Atmospheric Administration NOAA, the U.S. Department of Agriculture USDA, and the National Drought Mitigation Center (NDMC) at the University of Nebraska-Lincoln. The map is based on measurements of climatic, hydrologic, and soil conditions as well as reported impacts and observations from more than 350 contributors around the country. Eleven climatologists from the partner organizations take turns serving as the lead author each week. The authors examine all the data and use their best judgment to reconcile any differences in what different sources are saying. The analysts producing the map also weigh the indices according to how well they perform in various parts of the country and at different times of the year. Additional indicators are often needed in the West, where winter snowfall in the mountains has a strong bearing on water supplies. It is this combination of the best available data, local observations, and experts' best judgment that makes the U.S. Drought Monitor more versatile than other drought indicators.

Chapter 3

New storage-based drought index

3.1 Total Water Storage change from GRACE

GRACE has measured the time variable Earth's gravity field for about 15 years. We assume that most of the mass redistribution takes place within a thin layer of thickness H , including the portion of the atmosphere, oceans, ice caps, and below groundwater storage. Moreover, we pretend that this thin layer consists of water. As a result, the surface mass density can be converted into water height, commonly denoted as *Equivalent Water Height* (EWH) (Wahr et al., 1998):

$$\text{EWH}(\theta, \lambda) = \frac{a\rho_{\text{ave}}}{3\rho_{\text{w}}} \sum_{l=0}^{\infty} \frac{2l+1}{1+k_l} \sum_{m=0}^l \overline{P}_{l_m}(\cos\theta) [\overline{\Delta C}_{l_m} \cos m\lambda + \overline{\Delta S}_{l_m} \sin m\lambda], \quad (3.1)$$

where θ and λ are the co-latitude and longitude respectively. ρ_{w} is the average density of water ($= 1000 \text{ kg/m}^3$), ρ_{ave} is the average density of the Earth ($= 5517 \text{ kg/m}^3$), and k_l denote the degree-dependent load Love numbers used to account for the change in shape of the elastic Earth. \overline{P}_{l_m} are the fully normalized Legendre polynomials of degree l and order m while $\overline{\Delta C}_{l_m}$ and $\overline{\Delta S}_{l_m}$ are the fully normalized dimensionless spherical harmonic coefficients after subtracting the temporal mean. For more information about the derivation of water storage change from GRACE, see Appendix A.

The GRACE mission has released monthly gravity field solutions for ~ 15 years. Each solution consists of a set of spherical harmonic coefficients (SHs), C_{lm} and S_{lm} . They are provided by three GRACE data processing centers of the Science Data System (SDS), including the Center for Space Research (CSR) at the University of Texas at Austin, the Geoforschungszentrum (GFZ) in Potsdam, and the NASA Jet Propulsion Laboratory (JPL). Other groups (external to SDS) that also provide solutions include the Goddard Space Flight Center (NASA, Rowlands et al. (2002)), the Delft Institute of Earth Observation and Space Systems (DEOS; Klees et al. (2008)), the Institute of Geodesy (ifG) at the Graz University of Technology (ITSG, Kvas et al. (2019)), and others. Differences come from several issues including the background models used, the period over which the orbits are integrated, the weighting of the data, the maximum degree of the estimated gravity harmonics (Bettadpur, 2007; Flechtner, 2007; Watkins and Yuan, 2012). Temporal gravity field models developed by different institutions and agencies can be found at <http://icgem.gfz-potsdam.de/series> (last access: 1 October 2021). In this thesis, we have used the unconstrained solutions from ITSG-Grace2018 Kvas et al. (2019).

Figure 3.1 shows the scheme of the data processing used in this thesis to quantify TWSA using GRACE level-02 data. The processing includes:

- The lowest-degree zonal harmonic coefficients, C_{20} and C_{30} are replaced by the coefficients derived from Satellite Laser Ranging (SLR) data Cheng et al. (2013).
- The degree-1 coefficients are added to the GRACE fields of accounting for the movement of the Earth's center of mass Swenson et al. (2007).
- The Glacial Isostatic Adjustment (GIA) signal is corrected following AG and Zhong (2012).
- The SHs are corrected to ellipsoidal harmonics based on the method developed by Li et al. (2017) as the real shape of the Earth is more like an ellipsoid than a sphere.
- The primary (including S2, S1, and P1) and secondary (including M2, O2, O1, and Q1) residual tidal aliasing error are carefully removed following Tourian (2013).
- The long-term (2004–2010) mean of the SHs are subtracted as a representative of the static gravity field to calculate the geoid anomaly.

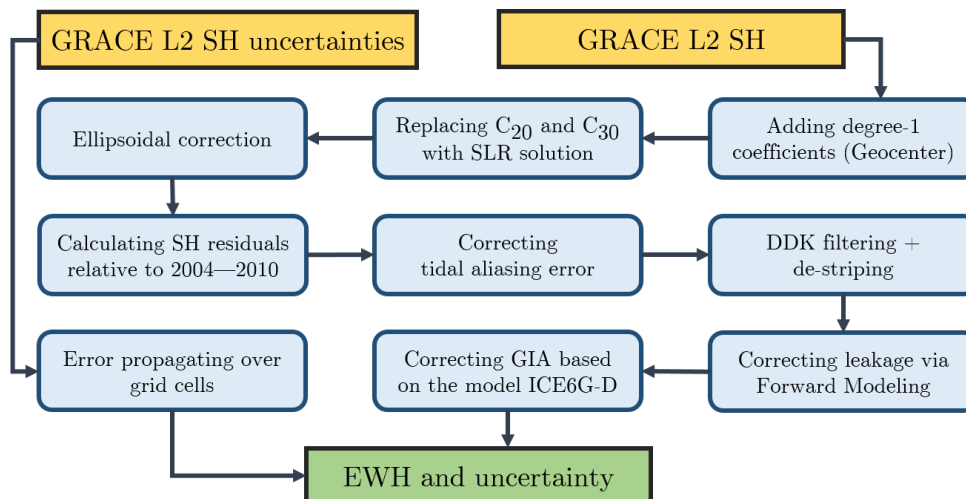


Figure 3.1: Flowchart of obtaining EWH in this thesis.

The monthly GRACE gravity field solutions suffer from correlated noise (cf. Figure 3.2) which comes from a range of random errors on the instrument data. Moreover, the maps of surface water height showed distinctive North-South striping patterns, because of GRACE's polar orbit configuration. There is a trade-off between the resolution and noise i.e., a higher (lower) degree of spherical harmonics coefficients would have larger (smaller) errors during the mission design. Therefore, one simple way to lower the noise would be to truncate the spherical harmonic series around degrees 20–30. However, for applications with high spatial resolution demand, such as hydrology, the monthly results include a complex noise.

The nature of the noise in GRACE is strongly anisotropic. In this thesis, we compared eight filter versions (denoted by DDK1 to DDK8) from the DDK anisotropic decorrelation filter developed by Kusche et al. (2009). Each version corresponds to different degrees of smoothing which decrease by the numbers in their names. The result for DDK3 is mainly used for

the drought analysis due to its better performance in eliminating the noises comparing to DDK4–DDK8. The filters DDK1 and DDK2 are ignored as they overfilter both noise and signal (cf. [Figure 3.3](#)). The gravity solutions in terms of spherical harmonic coefficients are truncated to degree/order 96 spanning the time interval April 2002–June 2017.

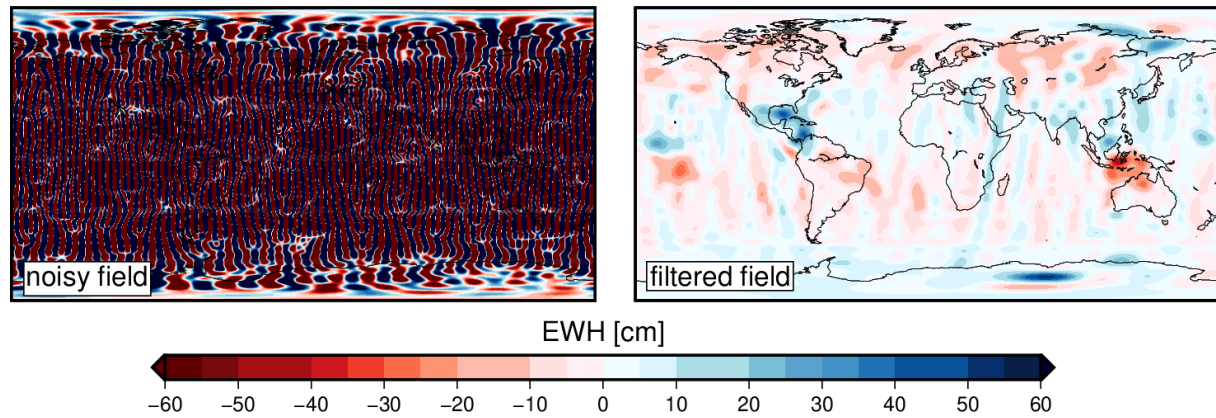


Figure 3.2: The GRACE EWH for October 2006, before and after filtering (DDK3).

Filtering results in leakage of signals. Therefore, to mitigate the leakage, we have used the forward modeling approach proposed by [Chen et al. \(2013\)](#). The final global fields of monthly EWH are retrieved from the residual coefficients, converted in to the $0.5^\circ \times 0.5^\circ$ grids. It is important to mention that the two neighboring grid cells are not completely *independent* due to the spatial smoothing filter. Finally, in order to achieve EWH time series for a region, the basin-scale time series is obtained as the weighted average of the GRACE EWH cell, with a weight proportional to the cell area falling within the basin boundary. [Figure 3.4](#) illustrates the time series of EWH over Tigris river basin located in the Middle East using the aforementioned DDK1 to DDK8 filters.

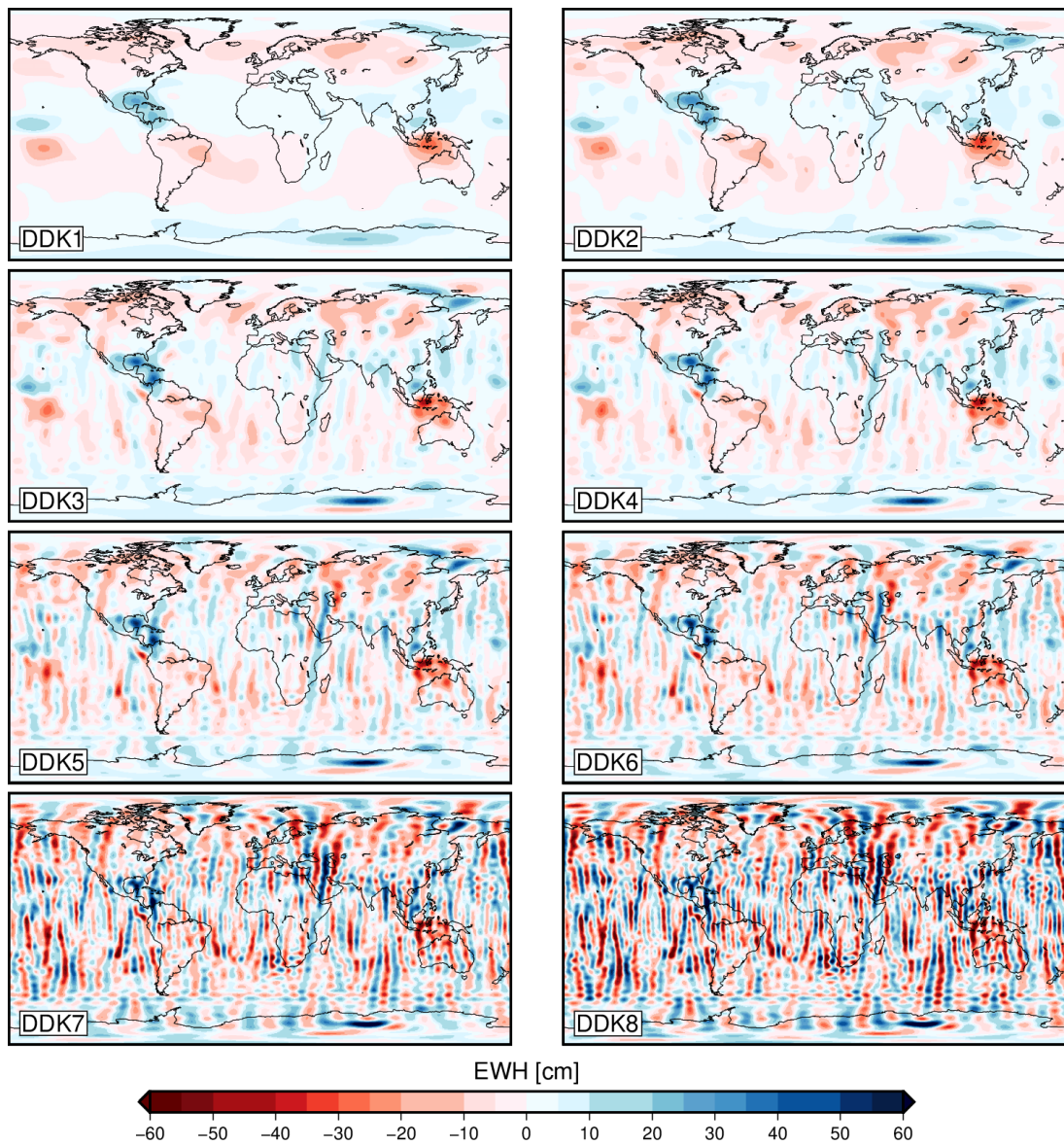


Figure 3.3: The GRACE EWH for April 2006, obtained from DDK1 to DDK8.

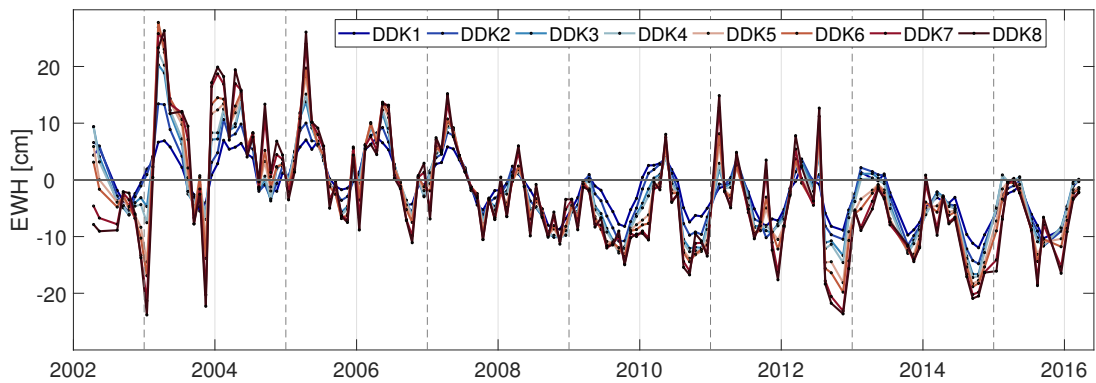


Figure 3.4: The GRACE EWH time series for the Tigris river basin in Iraq, obtained by applying DDK1 to DDK8 filters.

3.2 Total water storage deficits

Imagine that we have calculated the time series of EWH from GRACE for a region, e.g. [Figure 3.5](#)(top). From the perspective of drought identification, all parts of the time series that manifest water storage deficiency can represent a potential drought period. Therefore, we need a baseline to quantify the occurrence and severity of water storage deficits. One common approach to quantify this baseline is called *climatology*, e.g. ([Thomas et al., 2014](#)). The climatology represents the *normal* behavior of a region for a specific parameter related to the weather conditions. We can compute the monthly climatology for the GRACE EWH time series in each study region by averaging the values for each month of the satellite record (e.g., all Januaries in the ~ 15 -year record are averaged). Then, to quantify the deficiencies, we subtract the climatology from the GRACE EWH time series ([Figure 3.5](#)(middle)). We call the result EWH *anomalies* or EWHA, the negative values of which represent the water storage deficits. Characterizing drought will be finally to associate different categories of drought into the period which is colored in red in [Figure 3.5](#)(bottom). Before elaborate more on the final steps, in the following section, the possible choice of calculating the long-term monthly mean (climatology) is discussed.

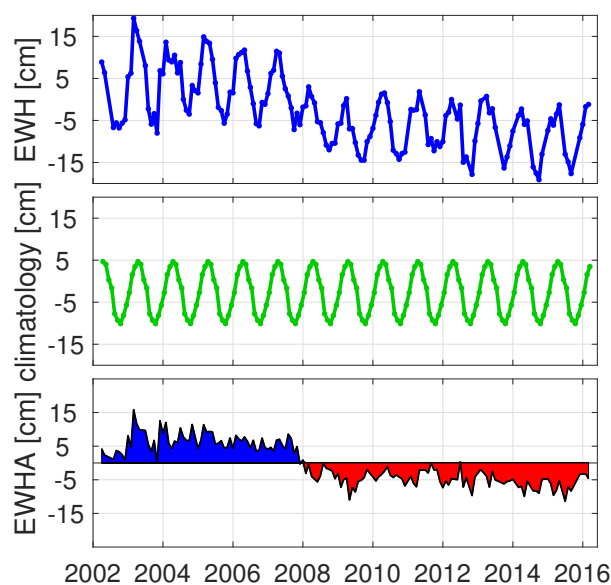


Figure 3.5: Time series of, Top:GRACE EWH, middle: climatology (obtained from the GRACE time period), and bottom: the GRACE EWH anomalies for the Tigris located in Iraq.

3.3 The short record of GRACE EWH

In contrast to *weather* which is the condition of the atmosphere over a brief period, *climate* represents the composite of day-to-day weather over a longer period. To establish a robust *Climatology*, a record of the climate variables for at least 30 years is preferable. Even 60 years of data might be needed to capture all the climate variations. However, the GRACE EWH period (2002–2016) is not long enough to capture the full range of wetness and dryness of a region

(Sun et al., 2017; Thomas et al., 2014; Wang and Russell, 2016). On one hand, agricultural areas have expanded in the last decade in several basins globally, which has led to a dramatic increase in groundwater extraction. This over-extraction has accelerated the negative trend in water storage in those regions. On the other hand, climate change in the same period has changed the pattern, intensity, and trend of the climate variables such as precipitation, temperature, and humidity. As a result, considering the period of GRACE (2002–2016) for the climatology calculation might lead to biased estimation.

Despite its importance, the effect of the short record of GRACE EWH time series on characterizing the storage-based drought has not been quantified. Only in the study by Zhao et al. (2017a), the standardized PDSI is compared within two periods, 2002–14 and 1982–2014. They found that the 13-year climatology will end up with underestimation (or overestimates) of the severity of the drought over 28% of their study domain (all land regions excluding Antarctica, Greenland, and barren ground). They suggest that stakeholders should correct the drought classification in these regions. Their study addressed the short record of data, however, the PDSI is sensitive to the change in the soil moisture which is only a fraction of the whole column of water. This implies that the comparison is blind to the change of groundwater and also surface runoff that includes a big portion of the EWH in many regions. Moreover, no minimum threshold for the time duration has been reported in the literature which would be sufficient to capture variations of the EWH in a region. The threshold might not be a single global fixed value, due to the different climate regions. As a result, any threshold would rather pursue a spatial distribution.

To compare the climatology within the GRACE period (2002–2016) with a longer period, we have used the ensemble mean of a group of models (EWH_L) including atmospheric models, global hydrological models, and land surface models (see section 3.4 for more details). Figure 3.6 shows the climatology of EWH over selected basins within three time periods, namely 1980–2016 (40 years), 2002–2016 (GRACE observation period), and 1980–2002 (pre GRACE). The difference between the climatology within 2002–2016 compared with a longer time period is undeniable throughout the whole year in basins that have experienced significant anthropogenic effects like groundwater extractions (like in Tigris, Death Valley, and the Ganges) or a dramatic climate change (like in Murray, Amazon, and Mackenzie). In other basins like Ob, Niger, or Mississippi the discrepancies mainly happen over cold months (October till February) while the warm months remain unchanged as we extend the sampling period for climatology. Figure 3.6 highlights the importance of longer sampling time for calculating the climatology. Moreover, the results reveal that the effect of the time period on the climatology will be basin-dependent and varies due to the geo-hydrological and climatological characteristics of each basin.

3.4 External climatology from models

In section 3.3 it is concluded that we need a longer time series of EWH than the GRACE observation period to calculate the climatology. One approach would be to reconstruct GRACE EWH time series. Humphrey et al. (2017) have reconstructed GRACE EWH using a statistical model based on two climate variables namely precipitation and temperature. Some other studies have assimilated GRACE observations into the hydrological models (Eicker et al., 2014; Kumar et al.,

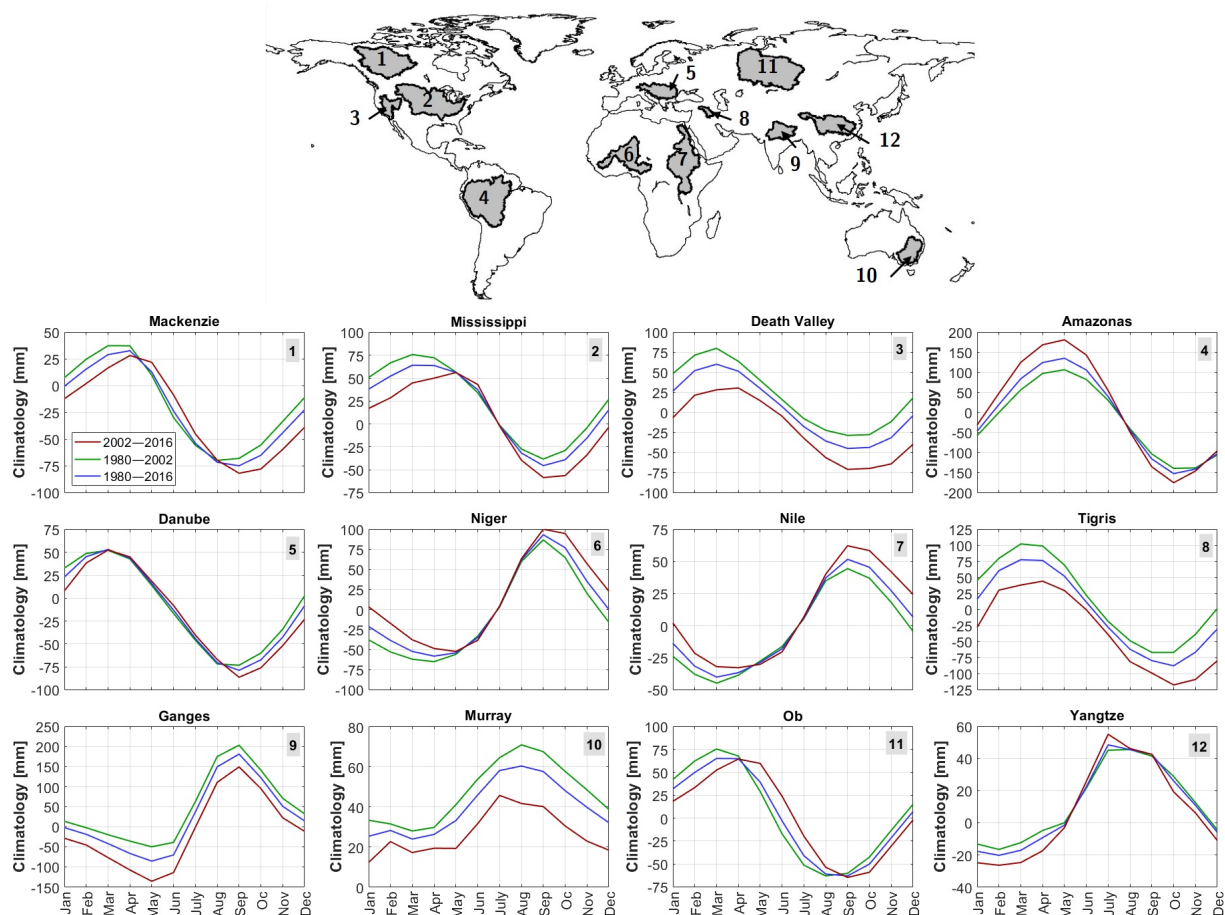


Figure 3.6: Long-term monthly mean (climatology) of EWH over selected basins within three periods namely 1980–2016 (40 years), 2002–2016 (GRACE observation period), and 1980–2002 (pre GRACE).

2016; Khaki et al., 2017; Schumacher et al., 2018). Recently, machine learning methods like the Long Short-Term Memory (LSTM) or Deep Neural Network (DNN) have been employed to reconstruct GRACE EWH at regional to global scales (Wang et al., 2021; Sun et al., 2020; Jing et al., 2020).

In this study, due to a lack of comprehensive study comparing these method, we propose an ensemble of the models listed in Table 3.1. We include Land Surface Models (LSMs), Global hydrological models, and atmospheric reanalysis models to calculate an ensemble mean. These models estimate EWH time series with a time period of at least 30 years are listed in the Table 3.1. The linear trend of the models are compared with three GRACE-based observations namely CSR GRACE RL06 Mascon solutions version 02 (Save, 2020; Save et al., 2016), JPL GRACE RL06 Mascon solutions version 02 (Wiese et al., 2019), and the approach proposed in ???. Based on the trend results, we conclude that the performance of the models varies globally and there is no superior model or small group of models among all. Therefore, in this study, we have untelized all models rather than selecting one or two among them.

To calculate the ensemble mean of the models, for each grid cell, first, we compare the Root Mean Squares (RMS) of the signal in the models within 2003–2012 (the insection between models and GRACE) with the corresponding value from GRACE EWH time series. Then, based on

Table 3.1: Summary of datasets used in this study.

Model	time period	Provider Organisation/Center	Reference
ERA5	1979–2016	ECMWF	Hersbach et al. (2020)
WGHM	1901–2016	Goethe University Frankfurt	Müller Schmied et al. (2021)
PCRGLOB-WB	1979–2012	Utrecht University	Wada et al. (2014) ; Sutanudjaja et al. (2018)
CLM5	1940–2014	ESG at NCAR	Lawrence et al. (2019)
HTESSEL	1979–2012	ECMWF	Balsamo et al. (2015)
JULES	1979–2012	CEH	Best et al. (2011) ; Clark et al. (2011)
LISFLOOD	1979–2012	JRC	Van Der Knijff et al. (2010)
ORCHIDEE	1979–2012	CNRS	Polcher et al. (2011)
SURFEX-TRIP	1979–2012	Meteo France	Decharme et al. (2013)
W3RA	1979–2012	CSIRO	Van Dijk (2010)
HBV-SIMREG	1979–2012	JRC	Lindström et al. (1997)

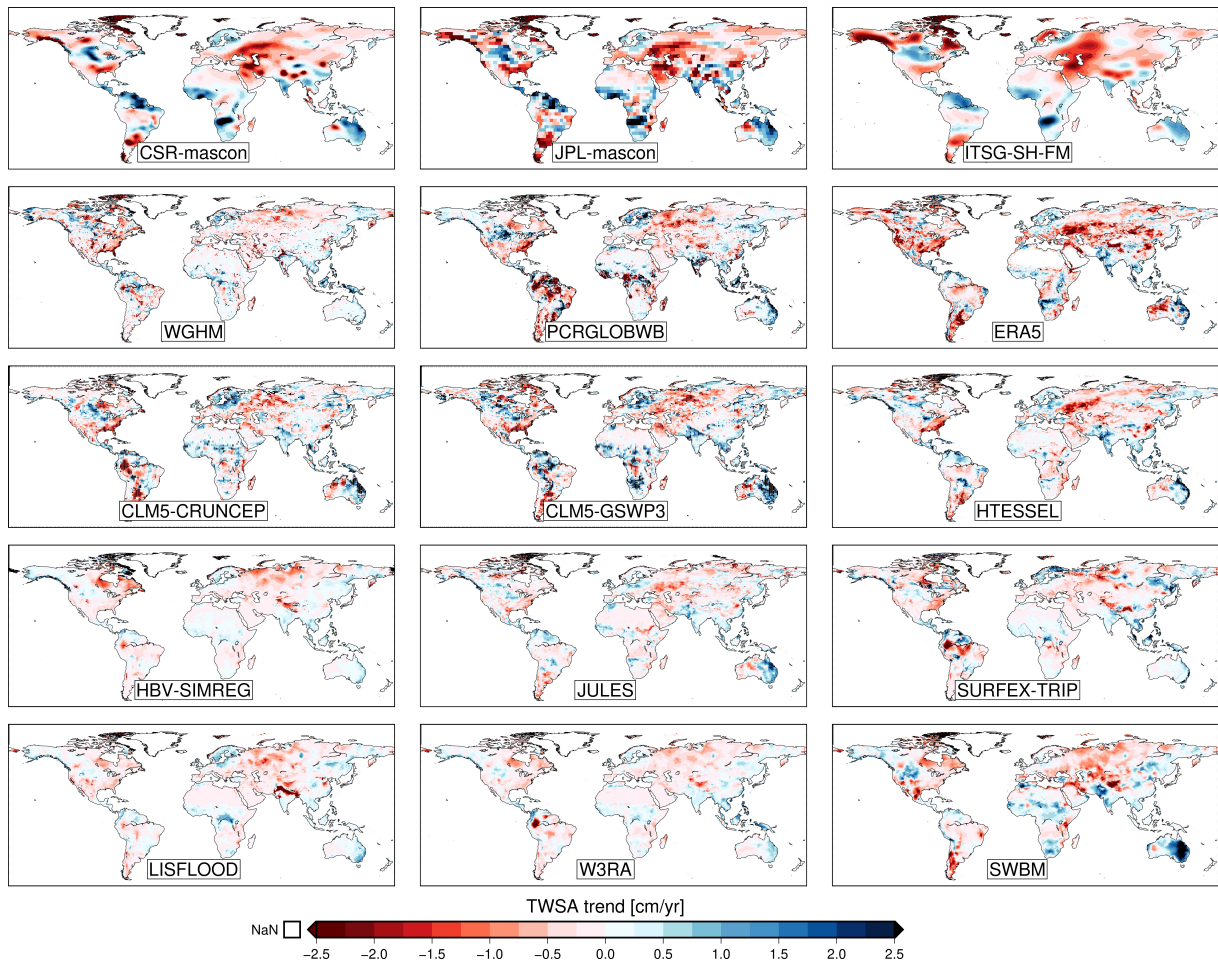


Figure 3.7: Linear trends obtained over the period 2002–2009 from the models.

the comparison, we select datasets with RMS difference of less than 30% of the GRACE EWH RMS. Finally, we calculate the ensemble mean of the selected datasets within 1980–2010. We use the new ensemble to calculate the climatology for each grid cell (or basin). [Figure 3.8](#) shows the

comparison between the ensemble mean of the selected models with GRACE EWH time series over selected basins.

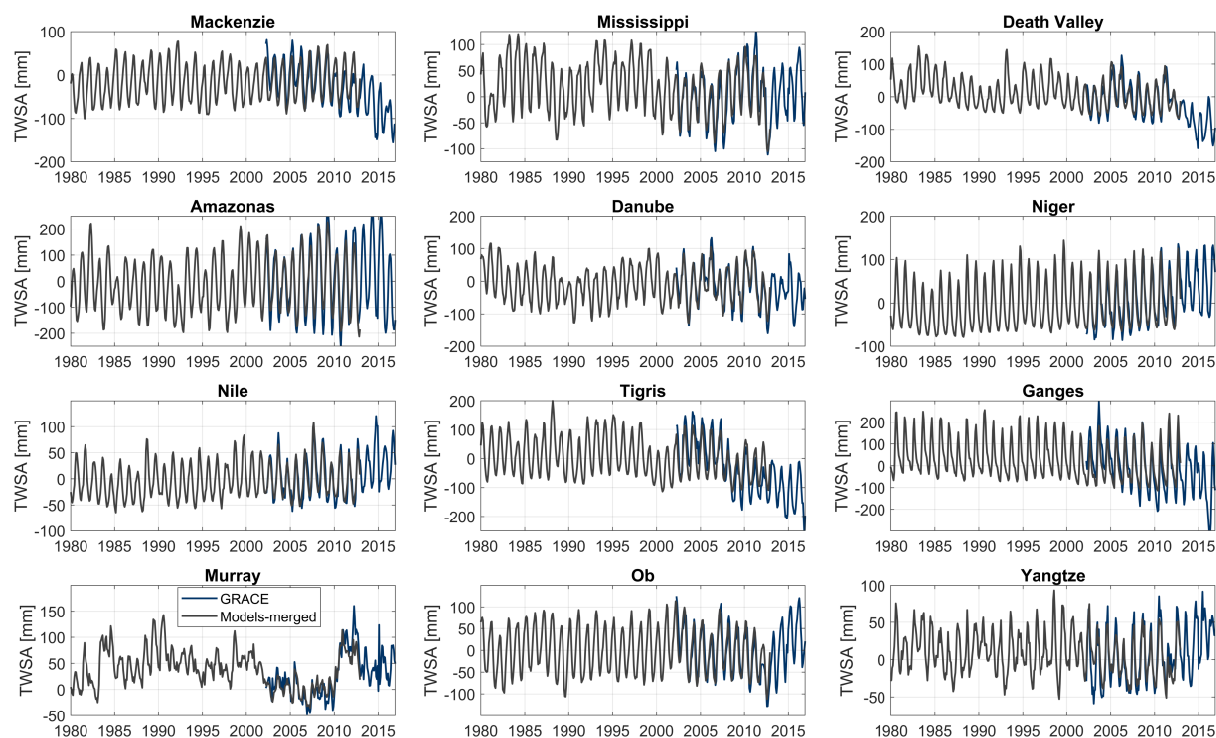


Figure 3.8: EWH time series from GRACE observations and the ensemble of the models for selected basins.

3.5 The storage-based drought index (SDI)

Step one we subtract the climatology from the GRACE EWH time series of each cell. We call the new time series the EWH anomaly EWhA. Negative values of the anomalies have the potential to be considered as drought. Two more subtle issues need to be considered before achieving the final formula for a Storage Based Drought Index (SDI):

- First, it happens sometimes in a region that the rainfall, that we expect to fall in a certain month, falls with one or two-month delay. This weather lateness cannot be considered as a drought. To address this concern, we accumulate the anomalies three months backward.
- Second, the GRACE EWH spatial resolution is coarse. Despite this coarse spatial resolution, each region may include a heterogeneous distribution of vegetation, climate variables (such as temperature, or rainfall.), and other compartments of the supply-demand balance of water. As a result, the range of humidity and aridity can change for that cells during the time period of GRACE (See [Zhao et al. \(2017b\)](#) for more details). To address this variation, we divide the three-month backward accumulated anomalies of each cell by its standard deviation during the whole time period of GRACE.

After considering two mentioned issues, for each grid cell, the dimensionless quantity of the SDI is defined as follow:

$$SDI_{i,j} = \frac{EWHA_{i,j} + EWHA_{i,j-1} + EWHA_{i,j-2}}{3\sigma_j} \quad (3.2)$$

where i is the year ranging from 2002 to 2016; j is the month ranging from January to December; and σ_j is the standard deviation of the residuals in month j . Figure shows the result of the calculation for EWHA and EWHA for the Tigris basin in Iraq.

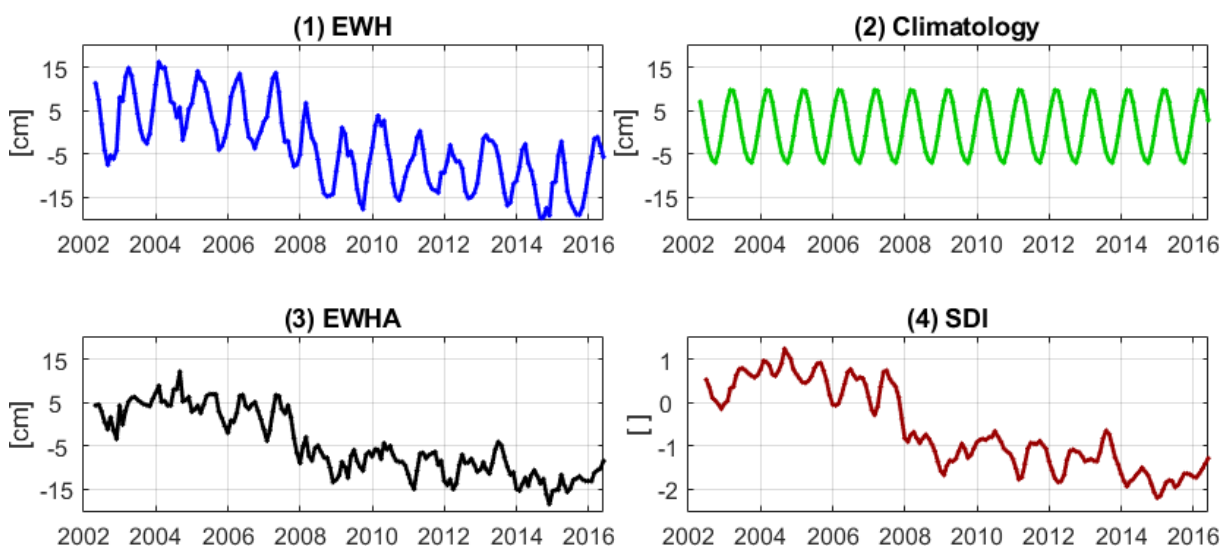







Figure 3.9: The 4 main steps in calculating SDI from the original EWH time series. Here the results are shown for the Tigris basin in Middle East.

Step two We classify drought into four levels of drought intensity (ranging from D1 to D4) and one level of "abnormal dryness" (D0) (Table 3.2). To make it consistent with other available drought maps, colors and percentile values are taken from the U.S. Drought Monitor (USDM), i.e., 30%, 20%, 10%, 5%, and 2% (Svoboda et al., 2002).

Table 3.2: USDM classification for drought characterization (Svoboda et al., 2002)

Category	Description	Color	Percentile range
D0	Abnormal dry		21–30
D1	Moderate drought		11–20
D2	Severe drought		6–10
D3	Extreme drought		3–5
D4	Exceptional drought		0–2

Lower and upper limits of the percentile range for each class of drought are calculated using the Cumulative Distribution Function (CDF) of the longer time series. To do that, first, we

calculated the CDF of SDI time series of the model. Then we investigated the best theoretical distribution function that fits with the empirical distribution. We examined more than 20 different distribution functions and calculated the error compared to the empirical distribution. Figure 3.10 shows the result of the comparison for the five best theoretical distribution functions and the errors for a cell inside the Tigris basin. Due to the high errors, we decided to directly employ the empirical CDF instead of fitting a theoretical function. Figure 3.11 presents the projection of the percentile ranges on the CDF obtained from the longer time series for a cell inside the Tigris basin. The class of drought for each month is defined using the quantile values from the empirical CDF.

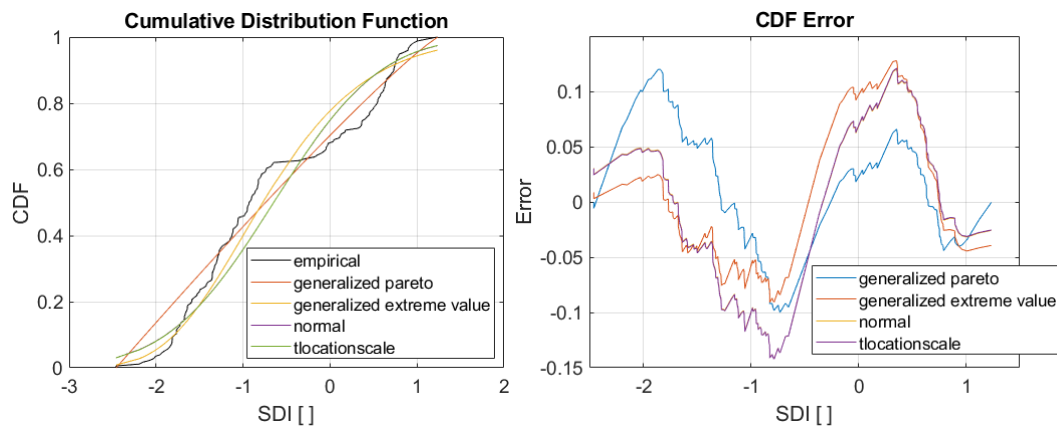


Figure 3.10: Left: The CDF distribution for the four best theoretical distribution functions (among 20 distribution functions) compared with empirical distribution. Tight: The related error in the three best best theoretical distribution compared with the empirical distribution

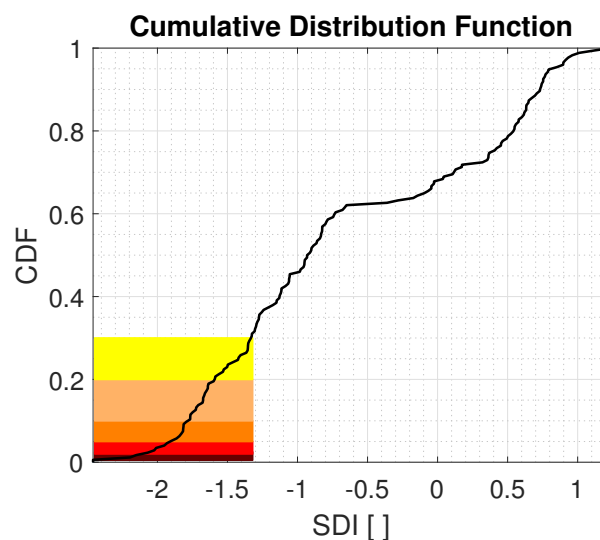


Figure 3.11: The projection of the percentile values for the different classes of drought on the empirical CDF of the long-time series of SDI for the Tigris basin. Quantile values will be then used for drought characterization

Chapter 4

Results and discussions

4.1 Global distribution of drought

Figure 4.1(a) shows the SDI over the global domain, excluding Antarctica and Greenland for July 2010, a month in which major drought conditions occurred worldwide (AghaKouchak, 2015). The drought map highlights severe to exceptional drought in western Russia, northern India, Amazon, Chile and Argentina, southeast Asia, eastern China, and central Africa. This is a global gridded storage-based drought map. Moreover, we calculated the global basin-scale SDI by aggregating the EWH from models and GRACE for each basin. Figure 4.1(b) presents the global basin-wide map for the same date as Figure 4.1(a). Figure 4.1 indicates that drought is a scale-dependent phenomenon.

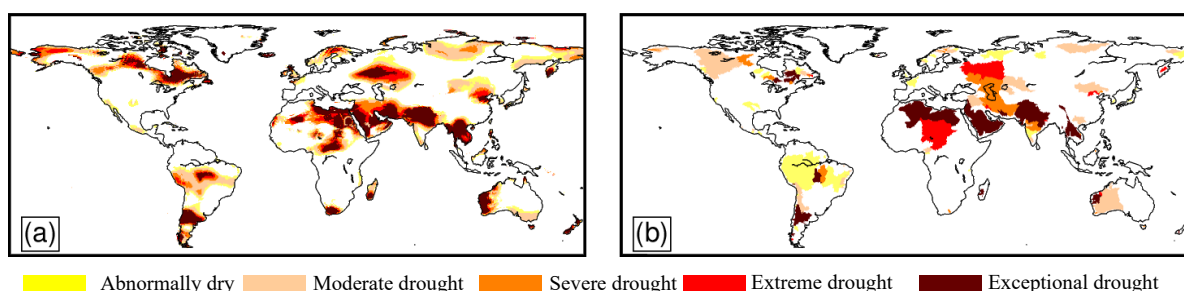


Figure 4.1: Global maps of drought characterization for July 2010, (a) gridded map and (b) basin-scale map.

Drought classes occur with different frequencies globally. We quantified the spatial distribution of the occurrence for each class of drought within the time period of the GRACE mission. Figure 4.2 shows the result for each class, from D1 to D4. Based on the result in Figure 4.2, some regions like Ogallala Aquifer in the United States, Northern India, Tigris and Euphrates basins in the Middle East, and eastern China have experienced more exceptional droughts during the last two decades. Most regions of the world have suffered at least one type of drought within 2002–2016.

4.2 Time evolution of drought for main catchments

Drought is a creeping phenomenon which evolves over time. We investigated the evolution of drought for 27 major basins within the time period of GRACE (cf. Figure 4.3). Some of the

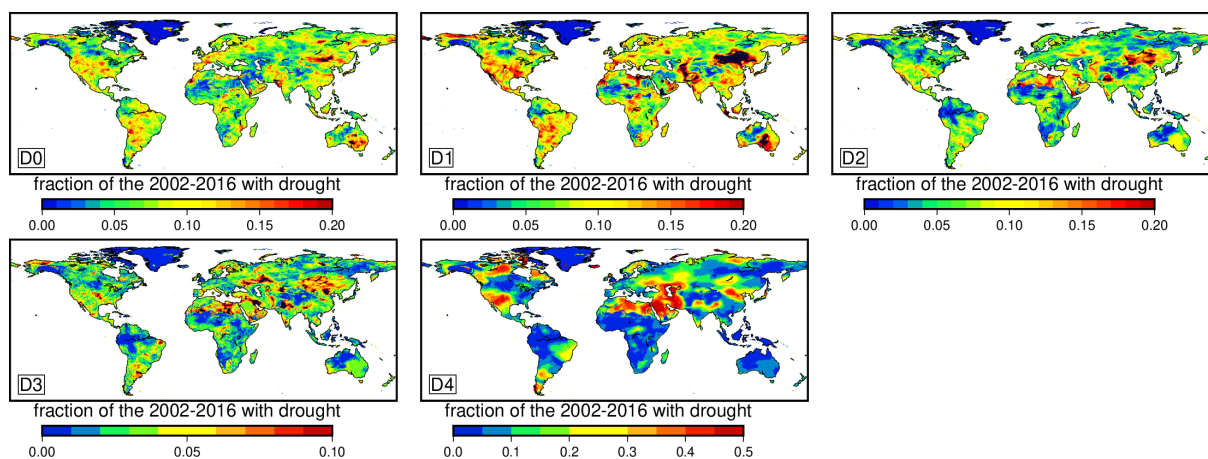


Figure 4.2: Spatial distribution of the frequency for each class of drought within the GRACE period (2002–2016).

basins suffered from more than one known drought period like Tigris and Euphrates in West Asia. Some of them are located in wet regions where we do not expect a drought period, like Amazon. Figure 4.3 shows the result for some selected basins. All the basins have suffered from different classes of drought in different periods. Some basins have experienced drought only for the first decade like Niger and Murray. In contrast, Tigris and Ganges, and Mackenzie have mostly suffered from drought in the second decade. The rest of the basins faced drought in different time periods of the whole time span. Some of the drought periods lasted just for a few months while some others stayed in a region for several months to several years, like Tigris.

4.3 Performance of the SDI during extreme hydrologic events

We evaluated the performance of the SDI results during some reported drought events during 2002–2016. Figure 4.4 shows SDI maps for selected parts of the world, each for specific dates:

Australia 2006 During October–December, Australia experienced one of the worst droughts on record (van Dijk et al., 2013).

Middle East 2012 A great part of Middle East suffered from drought (Gray, 2016; Saemian et al., 2020a).

Europe 2012 Southwestern Europe faced a significant drought during all seasons except Autumn. A lot of countries during this year experienced dry months compare to the last few decades including Germany, France, the United Kingdom, Portugal, and Spain (WMO, 2013).

North America 2012 By September approximately 64.6% of the United State suffered a moderate to exceptional drought (WMO, 2013).

South America 2010 Severe drought happened in southwestern of Amazon, the Mato Grosso state in Brazil, and north-central Bolivia (Lewis et al., 2011). It is reported that in October 2010, the Rio Negro river (one major tributary of the Amazon) experienced its lowest level since 1902 (Xu et al., 2011).

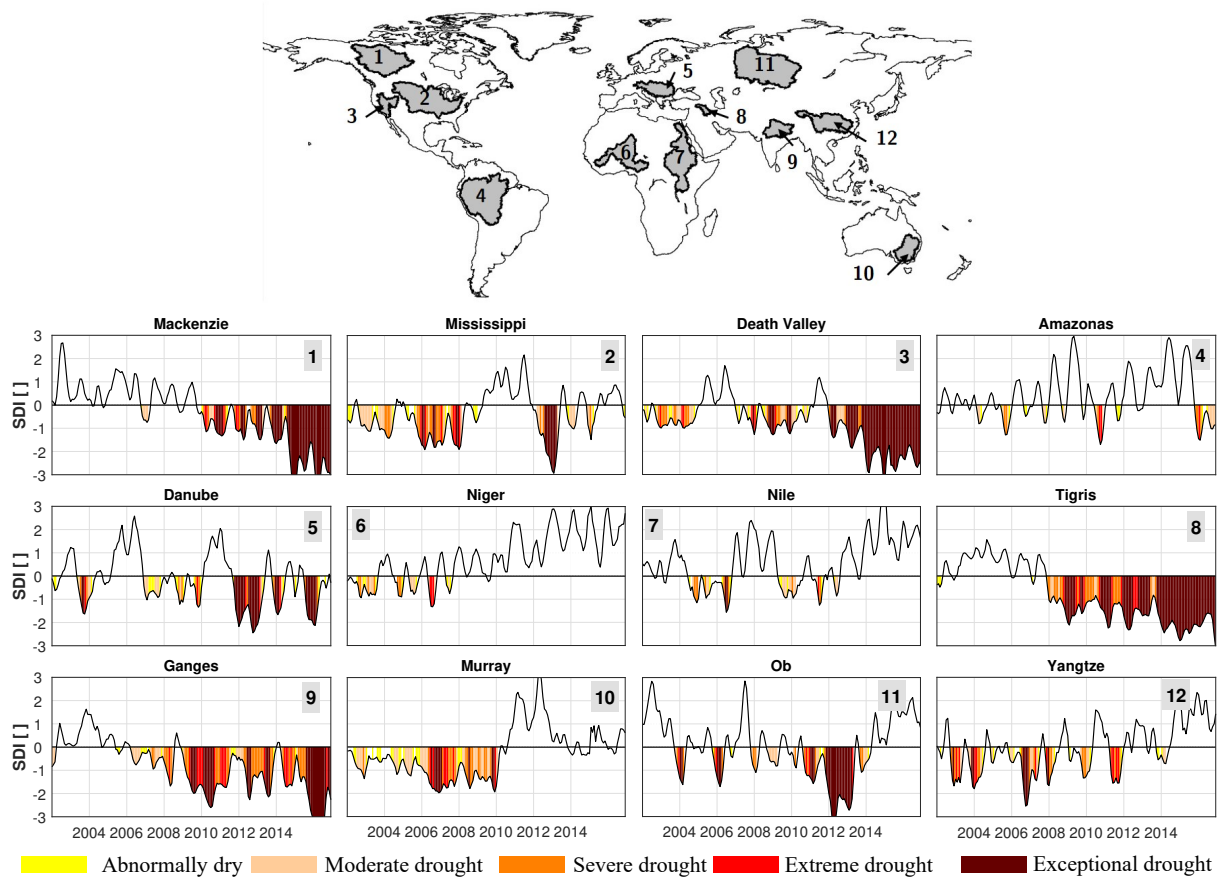


Figure 4.3: Time evolution of the SDI over selected basins.

Africa 2005 Southeastern Africa suffered a drought period (Guha-Sapir and Below, 2015).

All these documented droughts were captured well in the intensity and spatial distribution by SDI as is shown in Figure 4.4.

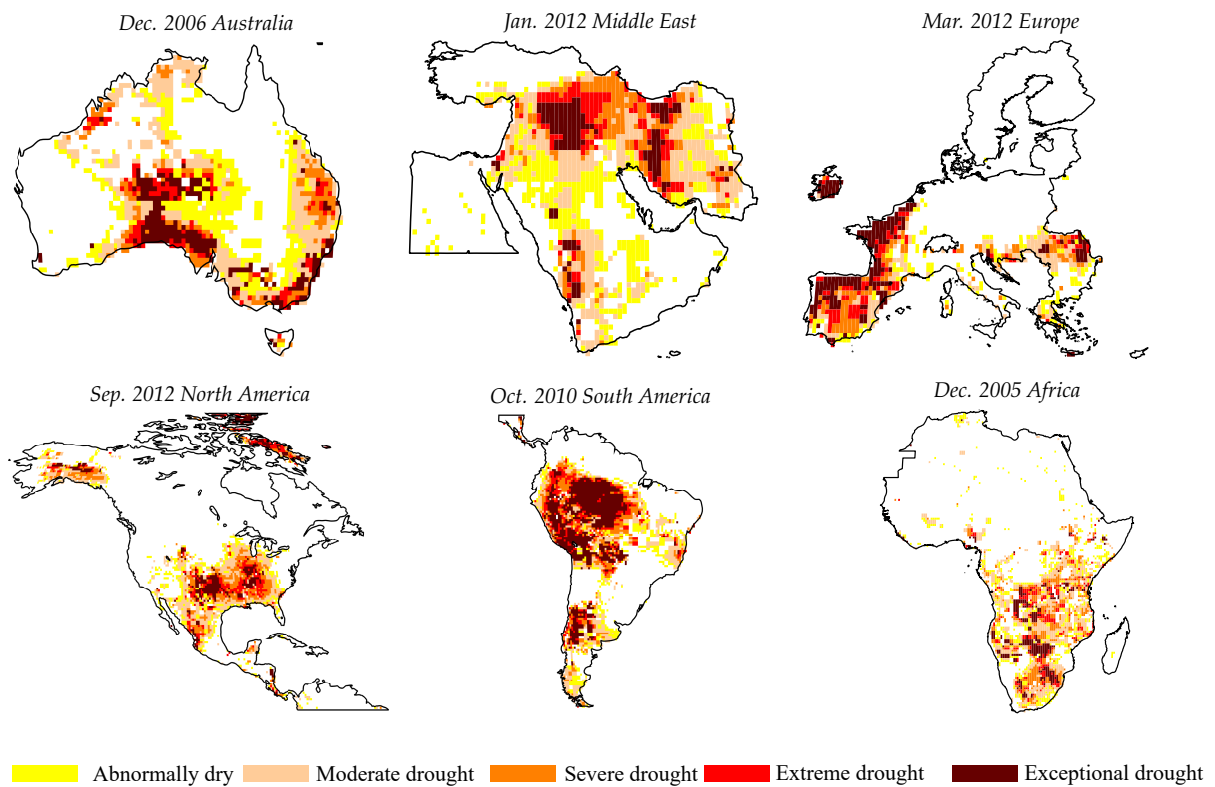


Figure 4.4: SDI results during some reported droughts.

4.4 Comparison of SDI with other drought indices

Figure 4.5 and Figure 4.6 show the time series of SDI over selected basins compared with SPI with different time scales (first column), SPEI with different time scales (second column), PDSI (third column). The last column shows the indices with the highest correlation at each column with SDI. Using the result from Rodell et al. (2018) (Figure 4.7), we have divided the selected basins in two groups. In the first group, Figure 4.5, the basins that have experienced considerable groundwater extraction have been selected. In the second group, Figure 4.6, we have selected basins with trend (positive or negative) from climate change (Ob, Niger and Mackenzie), basin with a considerable seasonal variation that has experienced both drought and floods (Amazonas), and finally Murray in Australia that is influenced via ENSO resulted in millinium drought.

Generally, the agreement between these two indices improves with the longer timescale. Over the first group, Figure 4.5 shows a reasonable agreement between SPI and SPEI before the negative trend while via the period with the considerable groundwater extractions, these two indices failed to capture the storage based drought. The main reason for poor correlation over these regions comes from the fact that the SPI relies only on precipitation while other water fluxes, such as evapotranspiration, groundwater, and ice and snow cover play key roles in the determination of the dry and wet conditions in these regions. While SPEI captures some human interventions signals via evapotranspiration, it still lacks the changes in groundwa-

ter and snow melting. SDI consider all the variation in the EWH and hence perform better over regions with significant anthropogenic effects. The PDSI on the other hand shows a better agreement comparing to SPI and SPEI while still failed to capture the dramatic negative trends in the EWH cause by the accelerated groundwater extraction within 2015–2016 in Death Valley, Yellow River, and Indus. The results suggest a notable contribution from SDI in detecting significant human groundwater withdraws while other drought indices miss the intensity of drought class.

In the second group (Figure 4.6), SPI and SPEI can capture the storage-based drought in regions where precipitation (with or without evapotranspiration) played the main role in the EWH variations, like Ob, Amazonas, and Murray basin. These basins were facing meteorological or agricultural rather than hydrological droughts over the study period. Like in the first group, the agreement between these two indices improves with the longer timescale. By increasing the time scale for calculating the SPI (or SPEI), the index reflects different phenomena from short-term soil moisture and crop stress to long-term precipitation patterns. Hence, the SPI-12 usually reveals the impact of drought on streamflows and even groundwater levels, which is more suitable for hydrological drought monitoring (WMO, 2012). The same story as the first group holds for Mackenzie but here instead of extreme groundwater extraction, the basin has observed a significant negative trend due to the ice-sheet loss (cf. Figure 4.7). The PDSI follows SDI in most basins except those with a considerable negative trend in Mackenzie and the positive trend in Niger.

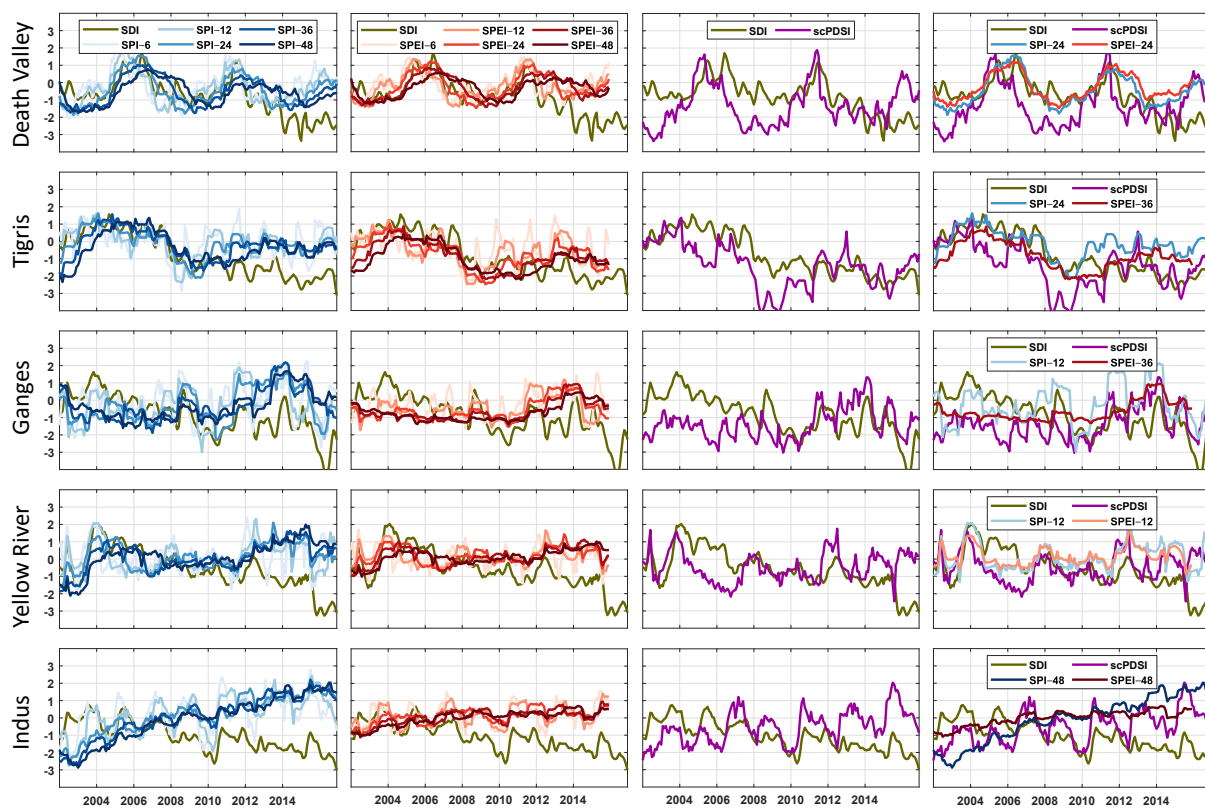


Figure 4.5: Comparison of drought indices namely SPI, SPEI, and PDSI with SDI over selected basins. The basins are located in regions with considerable groundwater extraction.

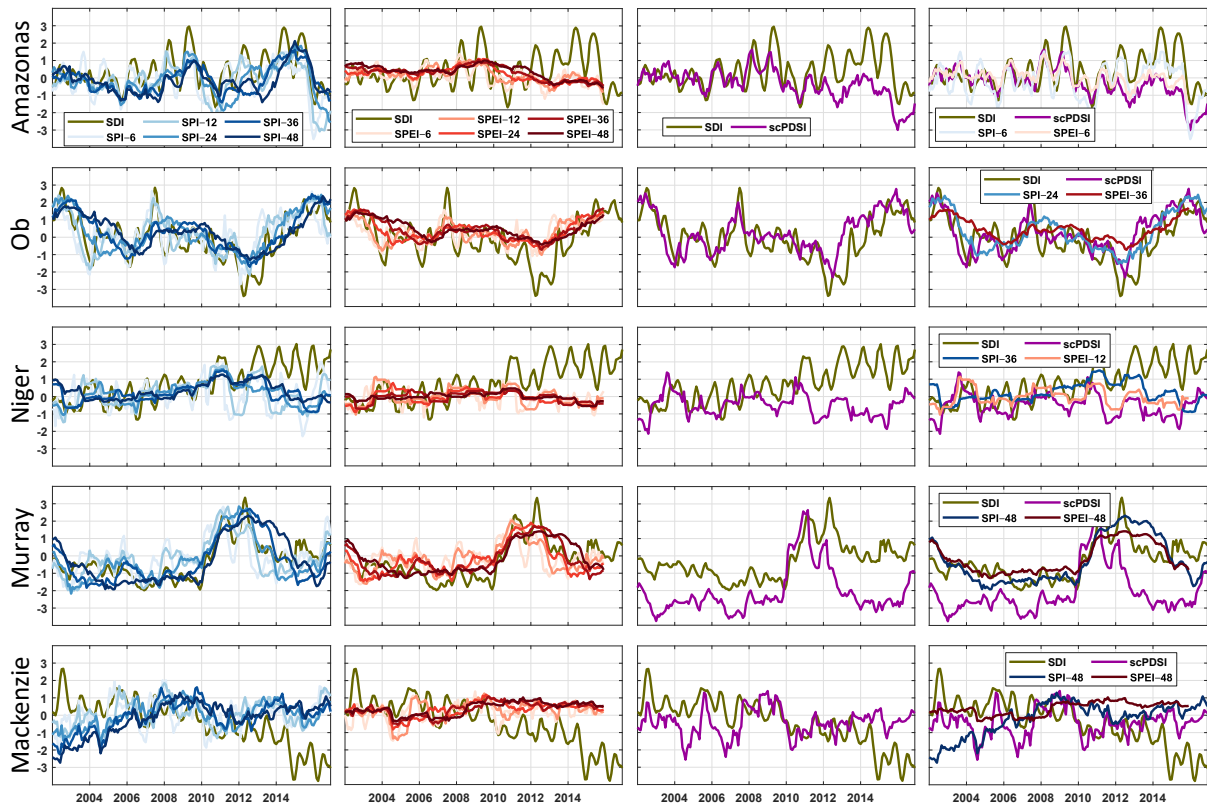


Figure 4.6: Comparison of drought indices namely SPI, SPEI, and PDSI with SDI over selected basins.

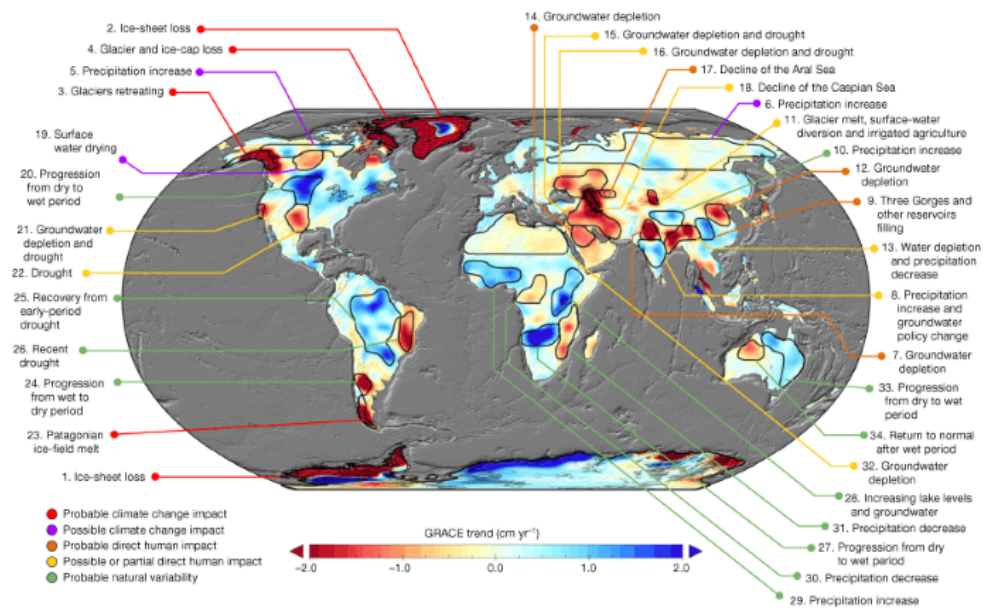


Figure 4.7: Trends in EWH (in centimetres per year) based on GRACE observations from April 2002 to March 2016 together with the possible interpretation over certain spots (Source: (Rodell et al., 2018)).

4.5 Comparison of SDI with USDM

We compared the result of SDI with the USDM maps for two recorded drought periods. The first event is the 2011 drought in Texas (Long et al., 2013). Figure 4.8 top shows drought characterization for August 2011, based on USDM and SDI. To examine the consequence of using only the short record of GRACE for *climatology*, we have shown the result of SDI using only GRACE EWH data as well. SDI captured the intensity and location of the drought in the Continental United States (CONUS) in general and in Texas. However, the short record of GRACE led to a miss-classification of the drought, although some similarities can be observed over some spots.

Throughout history, California has experienced many droughts, such as 1841, 1864, 1924, 1928–1935, 1947–1950, 1959–1960, 1976–1977, 2006–2010, and 2012–2017. We selected February 2016 as the middle of the last known drought periods in California. Figure 4.8 shows the result of drought characterization from the two aforementioned approaches. SDI captured the drought location and severity in California while the drought misclassified when using only the time record of GRACE. The comparison shows that SDI characterized exceptional drought over a larger extent than USDM. This might have happened since SDI is sensitive to all the variations in the water storage including the groundwater change, while the USDM does not take the deep water variations into account. In general, Figure 4.8 highlights the importance of the length of the EWH time series in the calculation of *climatology*.

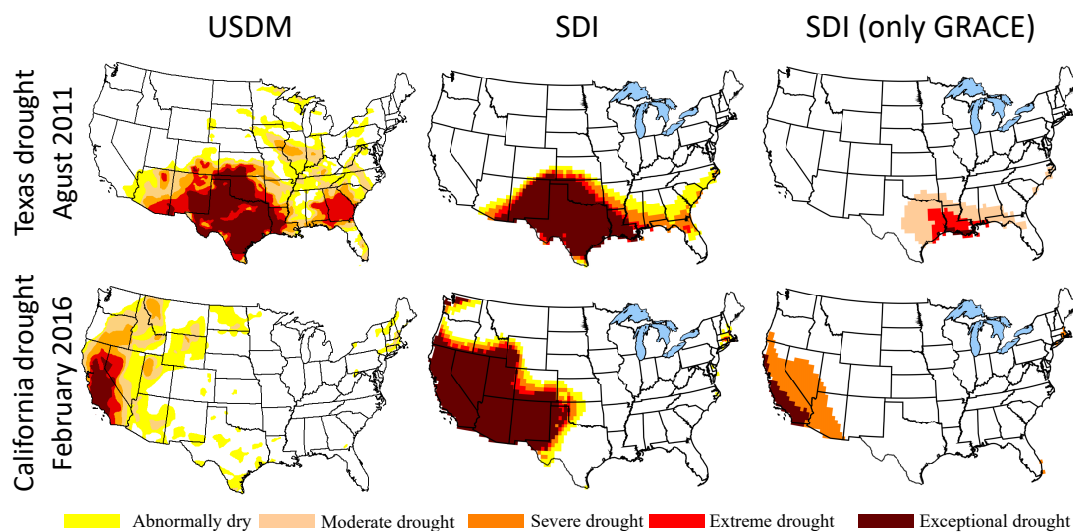


Figure 4.8: Drought classification from USDM, SDI, and SDI using only GRACE for the CONUS during August 2011 and February 2016.

4.6 Comparison of different approach for calculating SDI

In chapter 3, the methodology for calculating SDI is discussed. Generally, to calculate SDI we would reach crossroads twice. Once in deciding whether to remove trend in the EWH time series and the other time when we calculate climatology from the GRAC period or a longer time period. Figure 4.9 shows the comparison between:

- the approach proposed in this study (Figure 4.9 column (b))
- using only GRACE EWH for climatology while do not detrend the time series (Figure 4.9 column (c))
- using a longer period for calculating climatology but detrending the time series (Figure 4.9 column (d))

Three basins namely Death Valley, Tigris, and Mackenzie have experienced a dramatic negative trend in their EWH mainly in the second half of the last decade. The index proposed in this study can characterize drought in these regions while using only GRACE EWH for climatology will result in underestimating drought class and detrending the EWH time series shows periodic drought rather than a persistent significant water scarcity reported in those regions. The Yangtze river basin represents a region with no significant trend except for a weak positive trend in 2016. In this basin, generally, the discrepancies between different scenarios of calculating a storage-based drought index are minimal except for the last year where detrending EWH time series results in characterizing drought condition while the basin experience a wet year. Finally, the results over the Murray basin show that after detrending the millennium drought (2001–2009) can not be characterized and result in the mischaracterization of drought over the wet years (2010–2012) in this region. The GRACE period climatology would affect the severity and onset of the exceptional drought period. Figure 4.9 highlight the importance of longer time series for calculating climatology and depict the mischaracterization of drought by detrending the EWH time series.

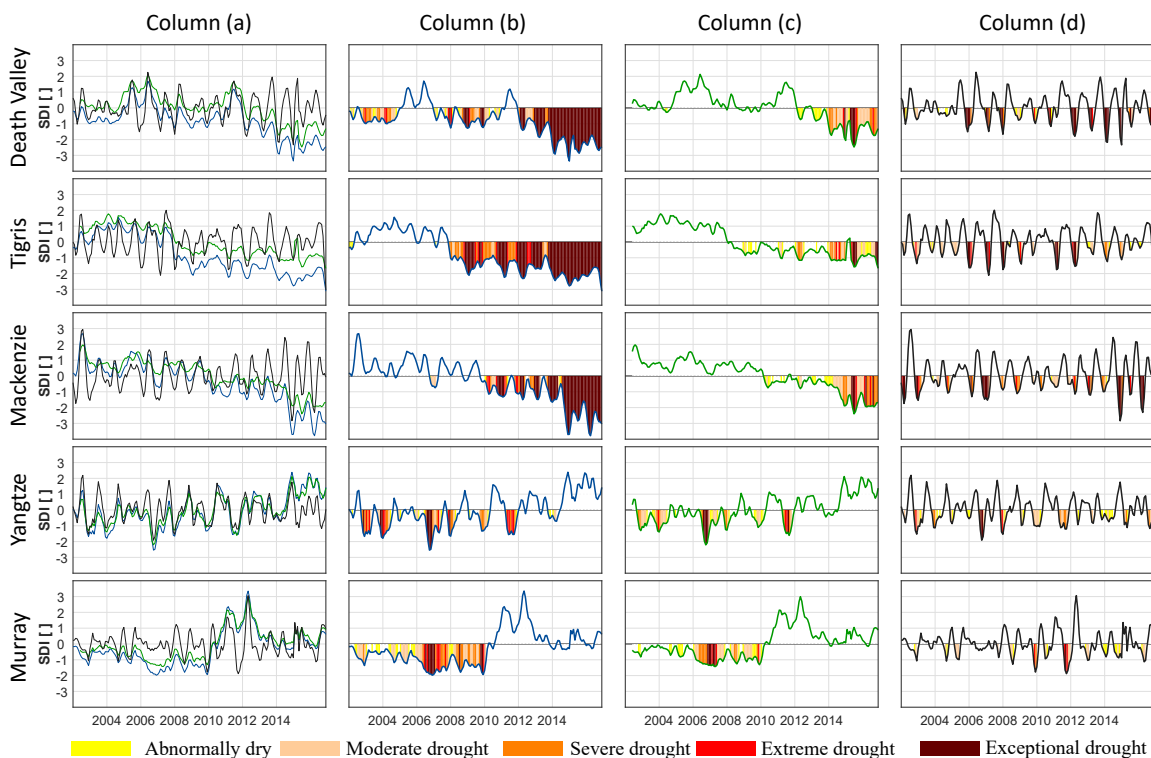


Figure 4.9: The storage-based drought index under different scenarios over selected basins: column (a) shows all together, column (b) illustrates the approach proposed in this study (SDI), column (c) depict the SDI but using GRACE climatology, and column (d) shows the SDI but over a detrended EWH.

Chapter 5

Summary and outlook

Drought is a compelling phenomenon happening globally at different climate zone with expanding negative economical, social, and political consequences. Monitoring drought at regional to global scale boosts our preparedness against the repercussions while enabling realistic risk assessments. Drought indices have been developed to summarize its complexity using quantitative approaches. Many drought indices have been developed so far using precipitation (e.g., SPI), precipitation and evapotranspiration (e.g., SPEI), and soil moisture (e.g., PDSI) to name but a few.

Since March 2002, the Gravity Recovery and Climate Experiment (GRACE) has measured the Earth's time-variable gravity field with unprecedented accuracy. The quantified redistribution of the mass within and among the Earth's atmosphere, oceans, land, and ice sheets from GRACE observation has made a quantum leap in hydrological applications. Monitoring extreme hydrological events like drought from GRACE measurements. In this study, we have investigated characterizing drought (i.e., its onset, duration, and severity) using satellite gravimetry observations. The introduction to drought and its fundamental differences with aridity and heatwaves have been discussed. To develop the new drought index, we have first quantified EWH from GRACE level 02 solutions. We have addressed the short record of GRACE time series for calculating the reference storage change, *climatology*, and quantified its importance over some selected basins. We found that the role of time series length for calculating climatology is significant over regions with considerable human intervention like extreme groundwater extractions in the Middle East or catchments with a considerable negative or positive trend mainly caused by climate change like the ice-melting over Mackenzie river basin in Canada or extreme precipitation events over Ob river basin as a boreal catchment.

Considering the vital need for a long (at least 30 years) record of EWH, we have extended GRACE observation back to 1980 using an ensemble of models (global hydrological models, land surface models, and atmospheric reanalysis models). The extended time series were then used to calculate climatology and percentile values. The results from the proposed SDI have presented both at gridded scale and basin-scale. Generally, The most extreme to exceptional storage-based droughts were observed over the Middle East, central Africa, northern India, mid and south America. The analysis from a different class of drought showed that most of the regions have suffered at least one type of drought within the study period (2002–2016). Exceptional drought frequency map showed the hot spots that have undergone significant negative trends via groundwater extractions like in the Middle East or exceptional shift in the precipitation pattern and intensity. The proposed SDI showed a considerable performance in

detecting some of the globally well-known documented droughts in terms of intensity and spatio-temporal distribution.

We have compared the storage-based drought with three most widely used drought indices namely SPI, SPEI, and PDSI. The results showed that the aforementioned indices follow SDI well over regions where the storage is driven by the climate rather than human activities. However, these indices failed to characterize drought over regions with significant human intervention like Tigris in the Middle East or Death Valley in the United States. In general, the correlation between the indices and SDI increases by the number of scales in their calculation. We have also investigated the consequence of using only GRACE EWH for climatology and detrending the time series before calculating the drought index. Both detrending and using the short record of GRACE would result in mischaracterizing drought, especially over regions with a considerable trend (positive or negative).

The comparison from the extended time series with the GRACE observation within 2002–2010 showed a considerable agreement. However, we did not compare our results with the other approaches to extend the GRACE observation like using the Machine Learning (ML) methods using hydrological and climatic variables. Moreover, GRACE EWH estimations include uncertainty that needs to be incorporated in characterizing storage-based drought ([Saemian et al., 2020b](#)). Finally, the successor of GRACE mission called GRACE Follow-On has been launched in May 2018 with about a year gap with GRACE. To have a continuous measurement of EWH and SDI this gap needs to be bridged.

Chapter 6

Appendixes

6.1 Satellite gravimetry applied to drought monitoring

The Earth's gravity is the sum of gravitational attraction and centrifugal force exerts on an object on or near its surface. It varies in strength and direction spatiotemporally. Thus, the Earth's gravity is a vector function of 3 coordinates or a vector field, taking the form of a not-quite-smooth ellipsoid. It consists of both static and time-variable components. The earlier includes the total mass of the Earth and mass heterogeneities and are orders of magnitude stronger. In the 1950s scientists including [Jeffries \(1952\)](#) addressed the time variable components (e.g., ocean tides that change gravitational potential). In principle, any mass displacements in, on or above the Earth manifest as variation in the gravity field.

The Earth's gravity field and its changes with time are used in various Earth-science related disciplines, such as geodesy, aerospace engineering, oceanography, climatology, and solid-Earth physics. The dynamic mechanism of the lithosphere, mantle convection, glacial isostatic adjustment (GIA), sea level change, hydrology, the mass balance of ice sheets and glaciers, and to name but a few, are some detailed applications ([Dickey et al., 1999](#); [Jin et al., 2010, 2011](#); [Simons and Hager, 1997](#); [Velicogna and Wahr, 2006](#); [Tapley et al., 2004](#)).

Three techniques have been used so far as classical measurements of Earth's gravity field. The first one is the surface gravity measurements (including terrestrial and airborne gravity data), works on the principle of measuring the constant downward acceleration of gravity ([Crossley et al., 2013](#)). Although the ground-based gravimeters measure the gravitational force (absolute or relative), the survey is costly and the labor work is hard. Moreover, the final result is more locally and the spatio-temporal resolution is low. The second technique employs the satellite radar altimetry measurements. Satellite altimetry measures the time taken by a radar pulse to travel from the satellite antenna to the surface and back to the satellite receiver. Combined with precise satellite location data, altimetry measurements yield sea-surface heights. This height empowers us to estimate the gravity field and the geoid over the ocean. Despite its revolutionized impact in sea-level measurements, the satellite altimetry still subject to various errors and spatio-temporal resolutions. The third technique utilizes laser ranging artificial Earth's satellite (also known as satellite gravimetry). The satellite gravimetry, excluding the difficulties of the two mentioned techniques, has greatly improved the gravity field precision and its application in geodesy, oceanography, hydrology, and geophysics. Incorporating all aforementioned techniques can give us the comprehensive gravity field models. The [Figure 6.1](#) shows a map of the static gravity field from one of the most recent solutions, the Earth's

Gravity Model 2008 (EGM08) (Pavlis et al., 2008).

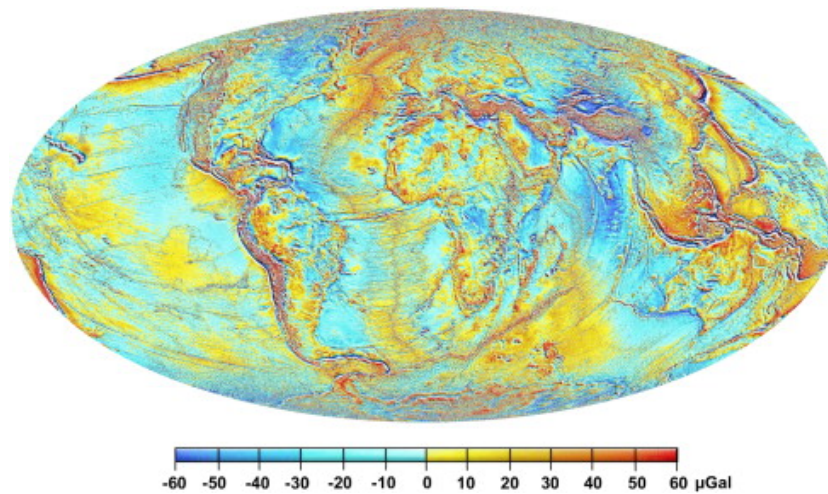


Figure 6.1: The static (average) Earth's gravity field (EGM08 model, from Pavlis et al. (2008)). Source: Bureau Gravimetric International.

In this chapter, first, a brief introduction about satellite gravimetry is discussed in section 6.2 followed by information about GRACE satellite mission in section 6.3. Equation 6.3 explains the derivation of terrestrial water storage from GRACE products (spherical harmonic coefficients).

6.2 Satellite gravimetry

Satellite gravimetry is a successful innovation and an outstanding breakthrough in the field of geodesy, following the Global Position System (GPS). Satellite orbital motion is largely affected by the gravitational force and other non-conservation forces. As a result, orbit solutions using a precise satellite tracking observation based on satellite laser ranging (SLR) enable us to estimate the Earth's gravity field. The laser pulse emits to a satellite, covered with reflectors. The run-trip travel time is measured after receiving the reflected pulse. We can determine the orbit using the sufficient amount of the position of the points (Wouters et al., 2014). Using this technique started with the Sputnik in 1957 and followed by the Laser Geodynamics Satellites (LAGEOS), launched in the 1970s and 1990s and still in operation today. However, satellite motion is determined not only by gravitational force but also by surface force (e.g., atmospheric drag and solar radiation pressure). As a result, all those satellites have to orbit the Earth at a high altitude (≈ 6000 km) to minimize the non-gravitational forces. However, the high altitude restricts the spatial resolution of the final Earth's gravity field typically to 10000 km (e.g., (Cheng et al., 1989; Rummel et al., 2002)).

The recent development of low-earth orbit (LEO) satellite gravimetry has significantly improved the Earth's gravity field model's precision and spatio-temporal resolution. Using LEO enabled scientists to provide global, regular and dense data sets of high and homogeneous

quality. Since 2000, three satellite missions have been launched and dedicated to the gravity field recovery, i.e., Challenging Mini-Satellite Payload (CHAMP; (Reigber et al., 2002)), Gravity Recovery and Climate Experiment (GRACE), and the Gravity Field and Steady-state Ocean Circulation Explorer (GOCE). Each of these three satellite mission follows one specific technique of tracking. These three techniques are as follow:

- High-low satellite to satellite tracking (hl-SST) (used for (CHAMP): In this mode, a low Earth orbiter is tracked by the high orbiting GPS and the satellites, relative to a network of ground stations. Moreover, non-gravitational forces on the low orbiter are measured by accelerometry (Figure 6.2a).
- High-low/low-low satellite to satellite tracking (hl-SST/ll-SST) (GRACE): In this mode, besides the hl-SST concept, the relative movement of two low and same orbiter satellite following each other is measured by an inter-satellite link (Figure 6.2b).
- High-low satellite to satellite tracking/satellite gravity gradient mode (GOCE): In this mode, in addition to the hl-SST concept, the acceleration differences between test-masses and the ensemble of them inside one low orbiting satellite are measured (Figure 6.2c).

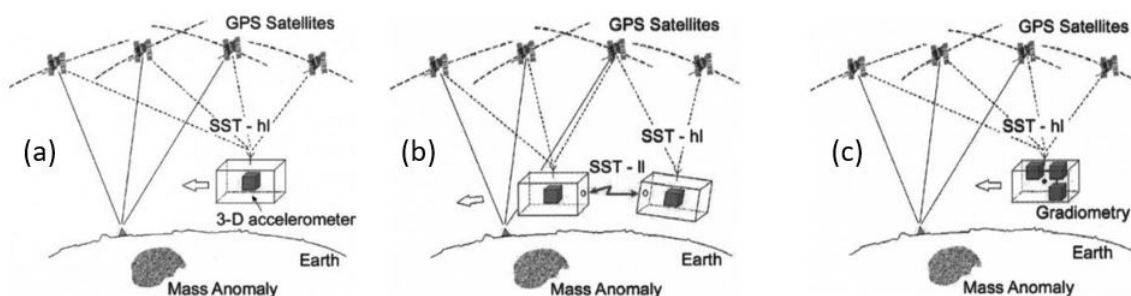


Figure 6.2: Concepts of: a: satellite-to-satellite tracking in the high-low mode (SST-hl); b: satellite-to-satellite tracking in the low-low mode (SST-ll) combined with SST-hl; c: satellite gradiometry combined with SST-hl

6.3 GRACE satellite mission

Since 2002, the US-German GRACE (Gravity Recovery and Climate Experiment) mission provided a precise survey of Earth's time-variable gravity field, with unprecedented temporal and spatial sampling down to the scales of a few hundred kilometers Tapley et al. (2004) (see Figure 6.3 for more details). The mission past the milestone of a 5-year design lifetime and produced data to near end of 2017. GRACE has measured and monitored monthly changes in how mass is redistributed within and among Earth's atmosphere, oceans, land and ice sheets, as well as within Earth itself. In the GRACE mission the higher resolution obtained by measuring the differential signal (demonstrates as changes in position and speed) between two satellite (test masses).

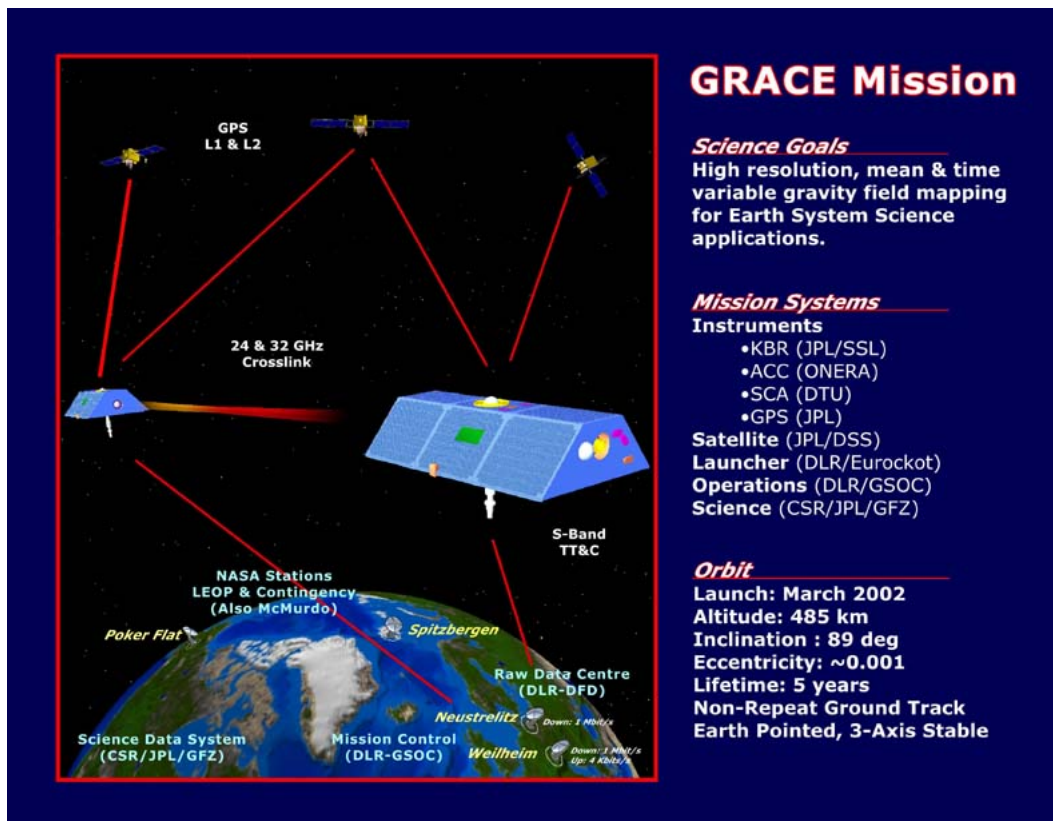


Figure 6.3: GRACE is a twin satellite mission orbiting the Earth at an initial altitude of about 500 km in a polar orbit (89°inclination), and 220 km apart (source: NASA).

The two GRACE satellites have completed about 15 years of continuous measurements. The mission followed by the Gravity Recovery and Climate Experiment Follow-On (GRACE-FO) mission, launched in May 22, 2018. The GRACE-FO will continue its predecessor mission by providing the Earth's time-variable gravity field, testing new technology. GRACE observations have been used in many scientific fields, ranging from verifying the "Lense-Thirring effect" of general relativity (Ciufolini et al., 2009) to detecting a giant meteorite impact underlain the Wilkes Land, Antarctica (von Frese et al., 2009), to even atmospheric science (Bruinsma et al., 2006; Bruinsma and Forbes, 2007). However, GRACE mainly enhanced our understanding of the Earth's subsystems (land, ocean, ice, and the solid Earth), correlating the mass redistribution with different components of the Earth's system.

6.4 Water storage change from GRACE

GRACE provided detailed measurement for Earth's gravity field commonly illustrated in terms of the shape of geoid: the equipotential surface corresponding to mean sea level over the oceans. The Earth's gravitational field is described by the geopotential V , using the following synthesis relation:

$$V(r, \theta, \lambda) = \frac{GM}{a_e} \left\{ \sum_{l=0}^{\infty} \sum_{m=0}^l \left(\frac{a_e}{r}\right)^{l+1} \overline{P}_{l_m}(\cos\theta) (C_{l_m} \cos m\lambda + S_{l_m} \sin m\lambda) \right\} \quad (6.1)$$

where G is the gravitational constant, M is the total mass of the Earth, a_e represent the mean equatorial radius of the Earth, r is the spherical coordinates radius, θ and λ are the co-latitude and longitude respectively. \overline{P}_{l_m} are the fully normalized Legendre polynomials of degree l and order m while C_{l_m} and S_{l_m} are the fully normalized dimensionless spherical harmonic coefficients, referred to as *Stokes coefficients* in geodesy. The \overline{P}_{l_m} can be calculated using the following equation:

$$\overline{P}_{l_m}(x) = \sqrt{(2 - \delta_{m0})(2l + 1) \frac{(l - m)!}{(l + m)!}} \times \frac{(1 - x^2)^{\frac{m}{2}}}{2^l l!} \frac{d^{l+m}}{dx^{l+m}} (x^2 - 1)^l \quad (6.2)$$

GRACE instead of a static gravity potential (Equation 6.1) provides the time-variable gravity information which is represented by change in the spherical harmonic coefficients. This variability can be seen as either the change in V from one time to the other, or the difference with respect to a time average of V . We considered the later interpretation and removed the long-term mean of spherical harmonic coefficients from monthly values. These residual spherical harmonic coefficients are denoted by ΔC_{l_m} and ΔS_{l_m} can be shown as follow, considering the density redistribution ($\Delta\rho(r, \theta, \phi)$) as the main cause of the geoid change:

$$\begin{Bmatrix} \Delta C_{l_m} \\ \Delta S_{l_m} \end{Bmatrix} = \frac{3}{4\pi a \rho_{ave} (2l + 1)} \int \int \int_v \Delta\rho(r, \theta, \lambda) \overline{P}_{l_m}(\cos\theta) \times \left(\frac{r}{a}\right)^{l+2} \begin{Bmatrix} \cos(m\lambda) \\ \sin(m\lambda) \end{Bmatrix} \sin\theta d\theta d\phi dr, \quad (6.3)$$

Where ρ_{ave} is the average density of the Earth ($= 5517 \text{ kg/m}^3$). We assume that most of the mass redistribution takes place within a thin layer of thickness H , including those portion of the atmosphere, oceans, ice caps, and below groundwater storage with significant mass fluctuations. When H is thin enough (i.e. $(l_{max} + 2)H/a \ll 1$) then $(\frac{r}{a})^{l+2}$ will be approximately equal to 1 and by replacing the volume integral of $\Delta\rho$ by the surface integral of $\Delta\sigma$ Equation 6.3 becomes:

$$\begin{Bmatrix} \Delta C_{l_m} \\ \Delta S_{l_m} \end{Bmatrix} = \frac{3}{4\pi a \rho_{ave} (2l + 1)} \int_{\Omega} \Delta\sigma(\theta, \lambda) \overline{P}_{l_m}(\cos\theta) \times \begin{Bmatrix} \cos(m\lambda) \\ \sin(m\lambda) \end{Bmatrix} d\Omega, \quad (6.4)$$

We can assume this thin layer consists of water. As a result, the surface mass density can be converted into water height, commonly denoted as *equivalent water height* (EWH) Wahr et al. (1998):

$$\text{EWH}(\theta, \lambda) = \rho_{\text{water}} \Delta\rho(\theta, \lambda) = \frac{a \rho_{ave}}{3 \rho_{\text{water}}} \sum_{l=0}^{\infty} \frac{(2l + 1)}{(1 + k_l)} \sum_{m=0}^l \overline{P}_{l_m}(\cos\theta) \times (\cos\theta) (C_{l_m} \cos m\lambda + S_{l_m} \sin m\lambda), \quad (6.5)$$

where ρ_{water} is the average density of water ($\rho_{\text{water}} = 1000\text{kg/m}^3$) and k_l is the Love number.

The GRACE Project has now released gravity field solutions for ~ 15 years. Each solution consists of a set of spherical harmonic coefficients, C_{lm} and S_{lm} . Monthly GRACE global gravity solutions are provided by three GRACE data processing centers of the Science Data System (SDS), including the Center for Space Research (CSR) at the University of Texas at Austin, the Geoforschungszentrum (GFZ) in Potsdam, and the NASA Jet Propulsion Laboratory (JPL). GRACE solutions are distributed by the NASA PODAAC (<http://podaac.jpl.nasa.gov/grace/>). Other groups (external to SDS) that also provide GRACE solutions include the Goddard Space Flight Center (NASA, [Rowlands et al. \(2002\)](#)), the Delft Institute of Earth Observation and Space Systems (DEOS; [Klees et al. \(2008\)](#)), the Groupe de Recherche de Geodesie Spatiale (GRGS, [Lemoine et al. \(2007\)](#)), the Institute of Theoretical Geodesy (ITG) at the University of Bonn ([Eicker et al. \(2008\)](#), 2008), and others. Differences in those aforementioned approaches of the processing centers comes from several issues including the background models used, the period over which the orbits are integrated, weighting of the data, the maximum degree of the estimated gravity harmonics, to name but a few ([Bettadpur \(2007\)](#); [Flechtner \(2007\)](#); [Watkins and Yuan \(2012\)](#)).

Bibliography

- W. J. AG and S. Zhong. Computations of the viscoelastic response of a 3-D compressible Earth to surface loading: an application to Glacial Isostatic Adjustment in Antarctica and Canada. *Geophys J Int*, 192(2):557–572, 2012. doi:[10.1093/gji/ggs030](https://doi.org/10.1093/gji/ggs030).
- A. AghaKouchak. Recognize anthropogenic drought. *Nature*, 524(7566):409, 2015. doi:[10.1038/524409a](https://doi.org/10.1038/524409a).
- W. M. Alley. The Palmer drought severity index: limitations and assumptions. *Journal of climate and applied meteorology*, 23(7):1100–1109, 1984. doi:[10.1175/1520-0450\(1984\)023<1100:TPDSIL>2.0.CO;2](https://doi.org/10.1175/1520-0450(1984)023<1100:TPDSIL>2.0.CO;2).
- G. Balsamo, C. Albergel, A. Beljaars, S. Boussetta, E. Brun, H. Cloke, D. Dee, E. Dutra, J. Muñoz-Sabater, F. Pappenberger, et al. ERA-Interim/Land: a global land surface reanalysis data set. *Hydrology and Earth System Sciences*, 19(1):389–407, 2015. doi:[10.5194/hess-19-389-2015](https://doi.org/10.5194/hess-19-389-2015).
- M. Best, M. Pryor, D. Clark, G. Rooney, R. Essery, C. Ménard, J. Edwards, M. Hendry, A. Porson, N. Gedney, et al. The Joint UK Land Environment Simulator (JULES), model description—Part 1: energy and water fluxes. *Geoscientific Model Development*, 4(3):677–699, 2011. doi:[10.5194/gmd-4-677-2011](https://doi.org/10.5194/gmd-4-677-2011).
- S. Bettadpur. CSR level-2 processing standards document for product release 04, GRACE 327-742, The GRACE Project. *Center for Space Research, University of Texas at Austin*, 2007.
- H. N. Bhalme and D. A. Mooley. Large-scale droughts/floods and monsoon circulation. *Monthly Weather Review*, 108(8):1197–1211, 1980. doi:[10.1175/1520-0493\(1980\)108<1197:LSDAMC>2.0.CO;2](https://doi.org/10.1175/1520-0493(1980)108<1197:LSDAMC>2.0.CO;2).
- J. P. Bruce. Natural disaster reduction and global change. *Bulletin of the American Meteorological Society*, 75(10):1831–1836, 1994. doi:[10.2307/26231430](https://doi.org/10.2307/26231430).
- S. Bruinsma, J. M. Forbes, R. S. Nerem, and X. Zhang. Thermosphere density response to the 20–21 November 2003 solar and geomagnetic storm from CHAMP and GRACE accelerometer data. *Journal of Geophysical Research: Space Physics*, 111(A6), 2006. doi:[10.1029/2005JA011284](https://doi.org/10.1029/2005JA011284).
- S. L. Bruinsma and J. M. Forbes. Storm-time equatorial density enhancements observed by CHAMP and GRACE. *Journal of Spacecraft and Rockets*, 44(6):1154–1159, 2007. doi:[10.2514/1.28134](https://doi.org/10.2514/1.28134).
- S. L. Castle, J. T. Reager, B. F. Thomas, A. J. Purdy, M.-H. Lo, J. S. Famiglietti, and Q. Tang. Remote detection of water management impacts on evapotranspiration in the Colorado River Basin. *Geophysical Research Letters*, 43(10):5089–5097, 2016. doi:[10.1002/2016GL068675](https://doi.org/10.1002/2016GL068675).

- F.-C. Chang and J. M. Wallace. Meteorological conditions during heat waves and droughts in the United States Great Plains. *Monthly Weather Review*, 115(7):1253–1269, 1987. doi:[10.1175/1520-0493\(1987\)115<1253:MCDHWA>2.0.CO;2](https://doi.org/10.1175/1520-0493(1987)115<1253:MCDHWA>2.0.CO;2).
- J. Chen, C. Wilson, B. Tapley, L. Longuevergne, Z. Yang, and B. Scanlon. Recent La Plata basin drought conditions observed by satellite gravimetry. *Journal of Geophysical Research: Atmospheres*, 115(D22), 2010. doi:[10.1029/2010JD014689](https://doi.org/10.1029/2010JD014689).
- J. Chen, C. Wilson, and B. Tapley. Contribution of ice sheet and mountain glacier melt to recent sea level rise. *Nature Geoscience*, 6(7):549–552, 2013. doi:[10.1038/ngeo1829](https://doi.org/10.1038/ngeo1829).
- J. Chen, J. S. Famiglietti, B. R. Scanlon, and M. Rodell. Groundwater storage changes: present status from GRACE observations. In *Remote Sensing and Water Resources*, pages 207–227. Springer, 2016. doi:[10.1007/s10712-015-9332-4](https://doi.org/10.1007/s10712-015-9332-4).
- M. Cheng, R. Eanes, C. Shum, B. Schutz, and B. Tapley. Temporal variations in low degree zonal harmonics from Starlette orbit analysis. *Geophysical Research Letters*, 16(5):393–396, 1989. doi:[10.1029/GL016i005p00393](https://doi.org/10.1029/GL016i005p00393).
- M. Cheng, B. D. Tapley, and J. C. Ries. Deceleration in the Earth’s oblateness. *Journal of Geophysical Research: Solid Earth*, 118(2):740–747, 2013. ISSN 2169-9356. doi:[10.1002/jgrb.50058](https://doi.org/10.1002/jgrb.50058).
- I. Ciufolini, A. Paolozzi, E. C. Pavlis, J. C. Ries, R. Koenig, R. A. Matzner, G. Sindoni, and H. Neumayer. Towards a one percent measurement of frame dragging by spin with satellite laser ranging to LAGEOS, LAGEOS 2 and LARES and GRACE gravity models. *Space Science Reviews*, 148(1-4):71–104, 2009. doi:[10.1007/s11214-009-9585-7](https://doi.org/10.1007/s11214-009-9585-7).
- D. Clark, L. Mercado, S. Sitch, C. Jones, N. Gedney, M. Best, M. Pryor, G. Rooney, R. Essery, E. Blyth, et al. The Joint UK Land Environment Simulator (JULES), model description—Part 2: carbon fluxes and vegetation dynamics. *Geoscientific Model Development*, 4(3):701–722, 2011. doi:[10.5194/gmd-4-701-2011](https://doi.org/10.5194/gmd-4-701-2011).
- D. Coumou and S. Rahmstorf. A decade of weather extremes. *Nature climate change*, 2(7):491, 2012. doi:[10.1038/nclimate1452](https://doi.org/10.1038/nclimate1452).
- D. Crossley, J. Hinderer, and U. Ricciardi. The measurement of surface gravity. *Reports on Progress in physics*, 76(4):046101, 2013. doi:[10.1088/0034-4885/76/4/046101](https://doi.org/10.1088/0034-4885/76/4/046101).
- B. Decharme, E. Martin, and S. Faroux. Reconciling soil thermal and hydrological lower boundary conditions in land surface models. *Journal of Geophysical Research: Atmospheres*, 118(14):7819–7834, 2013. doi:[10.1002/jgrd.50631](https://doi.org/10.1002/jgrd.50631).
- J. O. Dickey, C. R. Bentley, R. Bilham, J. A. Carton, R. J. Eanes, T. A. Herring, W. M. Kaula, G. S. Lagerloef, S. Rojstaczer, W. H. Smith, et al. Gravity and the hydrosphere: new frontier. *Hydrological sciences journal*, 44(3):407–415, 1999. doi:[10.1080/02626669909492236](https://doi.org/10.1080/02626669909492236).
- A. Eicker, M. Schumacher, J. Kusche, P. Döll, and H. M. Schmied. Calibration/data assimilation approach for integrating grace data into the watergap global hydrology model (wghm) using an ensemble kalman filter: First results. *Surveys in Geophysics*, 35(6):1285–1309, 2014. doi:[10.1007/s10712-014-9309-8](https://doi.org/10.1007/s10712-014-9309-8).
- A. Eicker et al. *Gravity field refinement by radial basis functions from in-situ satellite data*. Univ. Bonn, Inst. für Geodäsie und Geoinformation, 2008. URL <https://hdl.handle.net/20.500.11811/3245>.

- J. S. Famiglietti. Remote sensing of terrestrial water storage, soil moisture and surface waters. *The state of the planet: frontiers and challenges in geophysics*, pages 197–207, 2004. doi:[10.1029/150GM16](https://doi.org/10.1029/150GM16).
- F. Flechtner. AOD1B product description document for product releases 01 to 04 (Rev. 3.1, April 13, 2007). *GRACE project document*, pages 327–750, 2007.
- F. Frappart, G. Ramillien, S. Biancamaria, N. M. Mognard, and A. Cazenave. Evolution of high-latitude snow mass derived from the GRACE gravimetry mission (2002–2004). *Geophysical Research Letters*, 33(2), 2006. doi:[10.1029/2005GL024778](https://doi.org/10.1029/2005GL024778).
- E. Gray. NASA Finds Drought in Eastern Mediterranean Worst of Past 900 Years. <https://www.nasa.gov/feature/goddard/2016/nasa-finds-drought-in-eastern-mediterranean-worst-of-past-900-years>, 2016. Accessed: 2018-08-10.
- D. Guha-Sapir and R. Below. EM-DAT: International Disaster Database. <https://www.emdat.be/>, 2015. Accessed: 2018-08-10.
- J. Gutowski, C. Hegerl, J. Holland, R. Knutson, O. Mearns, J. Stouffer, J. Webster, F. Wehner, and W. Zwiars. Causes of observed changes in extremes and projections of future changes. *Weather and climate extremes in a changing climate, CCSP synthesis and assessment product 3.3*, 3:81–116, 2008.
- N. B. Guttman. Comparing the Palmer drought index and the standardized precipitation index 1. *JAWRA Journal of the American Water Resources Association*, 34(1):113–121, 1998. doi:[10.1111/j.1752-1688.1998.tb05964.x](https://doi.org/10.1111/j.1752-1688.1998.tb05964.x).
- J. Hansen, M. Sato, and R. Ruedy. Perception of climate change. *Proceedings of the National Academy of Sciences*, 109(37):E2415–E2423, 2012. doi:[10.1073/pnas.1205276109](https://doi.org/10.1073/pnas.1205276109).
- M. J. Hayes, M. D. Svoboda, D. A. Wihite, and O. V. Vanyarkho. Monitoring the 1996 drought using the standardized precipitation index. *Bulletin of the American meteorological society*, 80(3):429–438, 1999. doi:[10.1175/1520-0477\(1999\)080<0429:MTDUTS>2.0.CO;2](https://doi.org/10.1175/1520-0477(1999)080<0429:MTDUTS>2.0.CO;2).
- M. J. Hayes, O. V. Wilhelmi, and C. L. Knutson. Reducing drought risk: bridging theory and practice. *Natural Hazards Review*, 5(2):106–113, 2004. doi:[10.1061/\(asce\)1527-6988\(2004\)5:2\(106\)](https://doi.org/10.1061/(asce)1527-6988(2004)5:2(106)).
- H. Hersbach, B. Bell, P. Berrisford, S. Hirahara, A. Horányi, J. Muñoz-Sabater, J. Nicolas, C. Peubey, R. Radu, D. Schepers, et al. The ERA5 global reanalysis. *Quarterly Journal of the Royal Meteorological Society*, 146(730):1999–2049, 2020. doi:[10.1002/qj.3803](https://doi.org/10.1002/qj.3803).
- S. Hollinger, S. Isard, and M. Welford. A new soil moisture drought index for predicting crop yields. In *Preprints, Eighth Conference on Applied Climatology*, pages 187–190. American Meteorological Society Anaheim, CA, 1993.
- R. Houborg, M. Rodell, B. Li, R. Reichle, and B. F. Zaitchik. Drought indicators based on model-assimilated Gravity Recovery and Climate Experiment (GRACE) terrestrial water storage observations. *Water Resources Research*, 48(7), 2012. doi:[10.1029/2011WR011291](https://doi.org/10.1029/2011WR011291).
- V. Humphrey, L. Gudmundsson, and S. I. Seneviratne. A global reconstruction of climate-driven subdecadal water storage variability. *Geophysical Research Letters*, 44(5):2300–2309, 2017. doi:[10.1002/2017GL072564](https://doi.org/10.1002/2017GL072564).

- H. Jeffries. *The Earth: its origin, history and physical constitution*. Cambridge University Press, 1952.
- S. Jin, D. P. Chambers, and B. D. Tapley. Hydrological and oceanic effects on polar motion from GRACE and models. *Journal of Geophysical Research: Solid Earth*, 115(B2), 2010. doi:[10.1029/2009JB006635](https://doi.org/10.1029/2009JB006635).
- S. Jin, L. Zhang, and B. Tapley. The understanding of length-of-day variations from satellite gravity and laser ranging measurements. *Geophysical Journal International*, 184(2):651–660, 2011. doi:[10.1111/j.1365-246X.2010.04869.x](https://doi.org/10.1111/j.1365-246X.2010.04869.x).
- W. Jing, P. Zhang, X. Zhao, Y. Yang, H. Jiang, J. Xu, J. Yang, and Y. Li. Extending grace terrestrial water storage anomalies by combining the random forest regression and a spatially moving window structure. *Journal of Hydrology*, 590:125239, 2020. doi:[10.1016/j.jhydrol.2020.125239](https://doi.org/10.1016/j.jhydrol.2020.125239).
- P. Jones, K. Trenberth, P. Ambenje, R. Bojariu, D. Easterling, T. Klein, D. Parker, J. Renwick, M. Rusticucci, B. Soden, et al. Observations: surface and atmospheric climate change. *Climate change*, pages 235–336, 2007.
- M. Kassas. Aridity, drought and desertification. In *Arab environment. Future challenges*. Beirut, Lebanon: Arab Forum for Environment and Development, pages 95–110, 2008.
- M. Khaki, I. Hoteit, M. Kuhn, J. Awange, E. Forootan, A. I. Van Dijk, M. Schumacher, and C. Pattiaratchi. Assessing sequential data assimilation techniques for integrating grace data into a hydrological model. *Advances in Water Resources*, 107:301–316, 2017. doi:[10.1016/j.advwatres.2017.07.001](https://doi.org/10.1016/j.advwatres.2017.07.001).
- R. Klees, X. Liu, T. Wittwer, B. Gunter, E. Revtova, R. Tenzer, P. Ditmar, H. Winsemius, and H. Savenije. A comparison of global and regional GRACE models for land hydrology. *Surveys in Geophysics*, 29(4-5):335–359, 2008. doi:[10.1007/s10712-008-9049-8](https://doi.org/10.1007/s10712-008-9049-8).
- F. N. Kogan. Global drought watch from space. *Bulletin of the American Meteorological Society*, 78(4):621–636, 1997. doi:[10.1175/1520-0477\(1997\)078<0621:GDWFS>2.0.CO;2](https://doi.org/10.1175/1520-0477(1997)078<0621:GDWFS>2.0.CO;2).
- F. N. Kogan. Contribution of remote sensing to drought early warning. *Early warning systems for drought preparedness and drought management*, pages 75–87, 2000. doi:[10.1007/s10584-007-9283-y](https://doi.org/10.1007/s10584-007-9283-y).
- S. V. Kumar, B. F. Zaitchik, C. D. Peters-Lidard, M. Rodell, R. Reichle, B. Li, M. Jasinski, D. Mocko, A. Getirana, G. De Lannoy, et al. Assimilation of gridded grace terrestrial water storage estimates in the north american land data assimilation system. *Journal of Hydrometeorology*, 17(7):1951–1972, 2016. doi:[10.1175/JHM-D-15-0157.1](https://doi.org/10.1175/JHM-D-15-0157.1).
- J. Kusche, R. Schmidt, S. Petrovic, and R. Rietbroek. Decorrelated GRACE time-variable gravity solutions by GFZ, and their validation using a hydrological model. *Journal of geodesy*, 83(10):903–913, 2009. doi:[10.1007/s00190-009-0308-3](https://doi.org/10.1007/s00190-009-0308-3).
- A. Kvas, S. Behzadpour, M. Ellmer, B. Klinger, S. Strasser, N. Zehentner, and T. Mayer-Gürr. ITSG-Grace2018: Overview and evaluation of a new GRACE-only gravity field time series. *Journal of Geophysical Research: Solid Earth*, 124(8):9332–9344, 2019. doi:[10.1029/2019JB017415](https://doi.org/10.1029/2019JB017415).

- D. M. Lawrence, R. A. Fisher, C. D. Koven, K. W. Oleson, S. C. Swenson, G. Bonan, N. Collier, B. Ghimire, L. Van Kampenhout, D. Kennedy, et al. The Community Land Model version 5: Description of new features, benchmarking, and impact of forcing uncertainty. *Journal of Advances in Modeling Earth Systems*, 11(12):4245–4287, 2019. doi:[10.1029/2018MS001583](https://doi.org/10.1029/2018MS001583).
- J.-M. Lemoine, S. Bruinsma, S. Loyer, R. Biancale, J.-C. Marty, F. Perosanz, and G. Balmino. Temporal gravity field models inferred from GRACE data. *Advances in Space Research*, 39(10):1620–1629, 2007. doi:[10.1016/j.asr.2007.03.062](https://doi.org/10.1016/j.asr.2007.03.062).
- D. P. Lettenmaier and J. S. Famiglietti. Hydrology: Water from on high. *Nature*, 444(7119):562, 2006. doi:[10.1038/444562a](https://doi.org/10.1038/444562a).
- S. L. Lewis, P. M. Brando, O. L. Phillips, G. M. van der Heijden, and D. Nepstad. The 2010 Amazon drought. *Science*, 331(6017):554–554, 2011. doi:[10.1126/science.1200807](https://doi.org/10.1126/science.1200807).
- J. Li, J. Chen, Z. Li, S.-Y. Wang, and X. Hu. Ellipsoidal correction in GRACE surface mass change estimation. *Journal of Geophysical Research: Solid Earth*, 122(11):9437–9460, 2017.
- G. Lindström, B. Johansson, M. Persson, M. Gardelin, and S. Bergström. Development and test of the distributed HBV-96 hydrological model. *Journal of hydrology*, 201(1-4):272–288, 1997. doi:[10.1016/S0022-1694\(97\)00041-3](https://doi.org/10.1016/S0022-1694(97)00041-3).
- W. Liu and F. Kogan. Monitoring regional drought using the vegetation condition index. *International Journal of Remote Sensing*, 17(14):2761–2782, 1996. doi:[10.1080/01431169608949106](https://doi.org/10.1080/01431169608949106).
- B. Lloyd-Hughes and M. A. Saunders. A drought climatology for Europe. *International journal of climatology*, 22(13):1571–1592, 2002. doi:[10.1002/joc.846](https://doi.org/10.1002/joc.846).
- D. Long, B. R. Scanlon, L. Longuevergne, A. Y. Sun, D. N. Fernando, and H. Save. GRACE satellite monitoring of large depletion in water storage in response to the 2011 drought in Texas. *Geophysical Research Letters*, 40(13):3395–3401, 2013. doi:[10.1002/grl.50655](https://doi.org/10.1002/grl.50655).
- D. Long, L. Longuevergne, and B. R. Scanlon. Uncertainty in evapotranspiration from land surface modeling, remote sensing, and GRACE satellites. *Water Resources Research*, 50(2):1131–1151, 2014. doi:[10.1002/2013WR014581](https://doi.org/10.1002/2013WR014581).
- D. Long, L. Longuevergne, and B. R. Scanlon. Global analysis of approaches for deriving total water storage changes from GRACE satellites. *Water Resources Research*, 51(4):2574–2594, 2015. doi:[10.1002/2014WR016853](https://doi.org/10.1002/2014WR016853).
- T. B. McKee. Drought monitoring with multiple time scales. In *Proceedings of 9th Conference on Applied Climatology, Boston, 1995*, 1995.
- T. B. McKee, N. J. Doesken, J. Kleist, et al. The relationship of drought frequency and duration to time scales. In *Proceedings of the 8th Conference on Applied Climatology*, volume 17, pages 179–183. American Meteorological Society Boston, MA, 1993.
- G. A. Meehl, C. Tebaldi, G. Walton, D. Easterling, and L. McDaniel. Relative increase of record high maximum temperatures compared to record low minimum temperatures in the US. *Geophysical Research Letters*, 36(23), 2009. doi:[10.1029/2009GL040736](https://doi.org/10.1029/2009GL040736).
- A. Mehran, O. Mazdidasni, and A. AghaKouchak. A hybrid framework for assessing socio-economic drought: Linking climate variability, local resilience, and demand. *Journal of*

- Geophysical Research: Atmospheres*, 120(15):7520–7533, 2015. doi:[10.1002/2015JD023147](https://doi.org/10.1002/2015JD023147).
- S.-K. Min, X. Zhang, F. W. Zwiers, and G. C. Hegerl. Human contribution to more-intense precipitation extremes. *Nature*, 470(7334):378, 2011. doi:[10.1038/nature09763](https://doi.org/10.1038/nature09763).
- A. K. Mishra and V. P. Singh. A review of drought concepts. *Journal of hydrology*, 391(1-2): 202–216, 2010. doi:[10.1016/j.jhydrol.2010.07.012](https://doi.org/10.1016/j.jhydrol.2010.07.012).
- C. Mora, B. Dousset, I. R. Caldwell, F. E. Powell, R. C. Geronimo, C. R. Bielecki, C. W. Counsell, B. S. Dietrich, E. T. Johnston, L. V. Louis, et al. Global risk of deadly heat. *Nature Climate Change*, 7(7):501, 2017. doi:[10.1038/nclimate3322](https://doi.org/10.1038/nclimate3322).
- H. Müller Schmied, D. Cáceres, S. Eisner, M. Flörke, C. Herbert, C. Niemann, T. A. Peiris, E. Popat, F. T. Portmann, R. Reinecke, et al. The global water resources and use model WaterGAP v2. 2d: Model description and evaluation. *Geoscientific Model Development*, 14(2):1037–1079, 2021. doi:[10.5194/gmd-14-1037-2021](https://doi.org/10.5194/gmd-14-1037-2021).
- S. Niemeier et al. New drought indices. 80:267–274, 2008.
- G. Obasi. WMO’s role in the international decade for natural disaster reduction. *Bulletin of the American Meteorological Society*, 75(9):1655–1662, 1994.
- W. Palmer. Meteorological drought. US Department of Commerce Weather Bureau Research Paper No. 45, 1965.
- W. C. Palmer. Keeping track of crop moisture conditions, nationwide: The new crop moisture index. 1968.
- N. K. Pavlis, S. A. Holmes, S. C. Kenyon, and J. K. Factor. An earth gravitational model to degree 2160: EGM2008. *EGU General Assembly*, 2008(4):4–2, 2008.
- J. Polcher, N. Bertrand, H. Biemans, D. B. Clark, M. Floerke, N. Gedney, D. Gerten, T. Stacke, M. van Vliet, and F. Voss. Improvements in hydrological processes in general hydrological models and land surface models within WATCH. 2011.
- C. Reigber, H. Lühr, and P. Schwintzer. CHAMP mission status. *Advances in Space Research*, 30(2):129–134, 2002. doi:[10.1016/S0273-1177\(02\)00276-4](https://doi.org/10.1016/S0273-1177(02)00276-4).
- M. Rodell, J. Famiglietti, J. Chen, S. Seneviratne, P. Viterbo, S. Holl, and C. Wilson. Basin scale estimates of evapotranspiration using GRACE and other observations. *Geophysical Research Letters*, 31(20), 2004a. doi:[10.1029/2004GL020873](https://doi.org/10.1029/2004GL020873).
- M. Rodell, P. Houser, U. Jambor, J. Gottschalck, K. Mitchell, C. Meng, K. Arsenault, B. Cosgrove, J. Radakovich, M. Bosilovich, et al. The global land data assimilation system. *Bulletin of the American Meteorological Society*, 85(3):381–394, 2004b. doi:[10.1175/BAMS-85-3-381](https://doi.org/10.1175/BAMS-85-3-381).
- M. Rodell, I. Velicogna, and J. S. Famiglietti. Satellite-based estimates of groundwater depletion in India. *Nature*, 460(7258):999, 2009. doi:[10.1038/nature08238](https://doi.org/10.1038/nature08238).
- M. Rodell, J. S. Famiglietti, D. N. Wiese, J. Reager, H. K. Beaudoin, F. W. Landerer, and M.-H. Lo. Emerging trends in global freshwater availability. *Nature*, 557(7707):651–659, 2018. doi:[10.1038/s41586-018-0123-1](https://doi.org/10.1038/s41586-018-0123-1).
- D. D. Rowlands, R. D. Ray, D. S. Chinn, and F. G. Lemoine. Short-arc analysis of intersatellite tracking data in a gravity mapping mission. *Journal of Geodesy*, 76(6-7):307–316, 2002. doi:[10.1007/s00190-002-0255-8](https://doi.org/10.1007/s00190-002-0255-8).

- R. Rummel, G. Balmino, J. Johannessen, P. Visser, and P. Woodworth. Dedicated gravity field missions, principles and aims. *Journal of Geodynamics*, 33(1-2):3–20, 2002.
- S. Russo, J. Sillmann, and E. M. Fischer. Top ten European heatwaves since 1950 and their occurrence in the coming decades. *Environmental Research Letters*, 10(12):124003, 2015.
- P. Saemian, O. Elmi, B. Vishwakarma, M. Tourian, and N. Sneeuw. Analyzing the lake urchia restoration progress using ground-based and spaceborne observations. *Science of The Total Environment*, 739:139857, 2020a. doi:[10.1016/j.scitotenv.2020.139857](https://doi.org/10.1016/j.scitotenv.2020.139857).
- P. Saemian, M. Javad Tourian, and N. Sneeuw. The uncertainty of storage-based drought indices from grace. In *EGU General Assembly Conference Abstracts*, page 3604, 2020b.
- H. Save. CSR GRACE and GRACE-FO RL06 Mascon Solutions v02. 2020. Available online: http://www2.csr.utexas.edu/grace/RL06_mascons.html [Last accessed: 29 January 2021], 2020.
- H. Save, S. Bettadpur, and B. D. Tapley. High-resolution csr grace rl05 mascons. *Journal of Geophysical Research: Solid Earth*, 121(10):7547–7569, 2016. doi:[10.1002/2016JB013007](https://doi.org/10.1002/2016JB013007).
- B. R. Scanlon, Z. Zhang, R. C. Reedy, D. R. Pool, H. Save, D. Long, J. Chen, D. M. Wolock, B. D. Conway, and D. Winester. Hydrologic implications of GRACE satellite data in the Colorado River Basin. *Water Resources Research*, 51(12):9891–9903, 2015. doi:[10.1002/2015WR018090](https://doi.org/10.1002/2015WR018090).
- M. Schumacher, E. Forootan, A. I. van Dijk, H. M. Schmied, R. S. Crosbie, J. Kusche, and P. Döll. Improving drought simulations within the murray-darling basin by combined calibration/assimilation of grace data into the watergap global hydrology model. *Remote Sensing of Environment*, 204:212–228, 2018. doi:[10.1016/j.rse.2017.10.029](https://doi.org/10.1016/j.rse.2017.10.029).
- F. Seitz, M. Schmidt, and C. Shum. Signals of extreme weather conditions in Central Europe in GRACE 4-D hydrological mass variations. *Earth and Planetary Science Letters*, 268(1-2): 165–170, 2008. doi:[10.1016/j.epsl.2008.01.001](https://doi.org/10.1016/j.epsl.2008.01.001).
- B. Shafer. Developemnet of a surface water supply index (SWSI) to assess the severity of drought conditions in snowpack runoff areas. In *Proceedings of the 50th Annual Western Snow Conference, Colorado State University, Fort Collins, 1982*, 1982.
- M. Simons and B. H. Hager. Localization of the gravity field and the signature of glacial rebound. *Nature*, 390(6659):500, 1997. doi:[10.1038/37339](https://doi.org/10.1038/37339).
- A. Y. Sun, R. Green, S. Swenson, and M. Rodell. Toward calibration of regional groundwater models using GRACE data. *Journal of Hydrology*, 422:1–9, 2012. doi:[10.1016/j.jhydrol.2011.10.025](https://doi.org/10.1016/j.jhydrol.2011.10.025).
- A. Y. Sun, B. R. Scanlon, A. AghaKouchak, and Z. Zhang. Using GRACE Satellite gravimetry for assessing large-scale hydrologic extremes. *Remote Sensing*, 9(12):1287, 2017. doi:[10.3390/rs9121287](https://doi.org/10.3390/rs9121287).
- Z. Sun, D. Long, W. Yang, X. Li, and Y. Pan. Reconstruction of grace data on changes in total water storage over the global land surface and 60 basins. *Water Resources Research*, 56(4): e2019WR026250, 2020. doi:[10.1029/2019WR026250](https://doi.org/10.1029/2019WR026250).
- E. H. Sutanudjaja, R. Van Beek, N. Wanders, Y. Wada, J. H. Bosmans, N. Drost, R. J. Van Der Ent, I. E. De Graaf, J. M. Hoch, K. De Jong, et al. PCR-GLOBWB 2: a 5 arcmin global hydro-

- logical and water resources model. *Geoscientific Model Development*, 11(6):2429–2453, 2018. doi:[10.5194/gmd-11-2429-2018](https://doi.org/10.5194/gmd-11-2429-2018).
- M. Svoboda, D. LeComte, M. Hayes, R. Heim, K. Gleason, J. Angel, B. Rippey, R. Tinker, M. Palecki, D. Stooksbury, et al. The drought monitor. *Bulletin of the American Meteorological Society*, 83(8):1181–1190, 2002. doi:[10.1175/1520-0477-83.8.1181](https://doi.org/10.1175/1520-0477-83.8.1181).
- S. Swenson, D. Chamber, and J. Wahr. Estimating geocenter variations from a combination of GRACE and ocean model output. *Journal of Geophysical Research*, 113:B08410, 2007. doi:[10.1029/2007JB005338](https://doi.org/10.1029/2007JB005338).
- T. Syed, J. Famiglietti, J. Chen, M. Rodell, S. I. Seneviratne, P. Viterbo, and C. Wilson. Total basin discharge for the Amazon and Mississippi River basins from GRACE and a land-atmosphere water balance. *Geophysical Research Letters*, 32(24), 2005. doi:[10.1029/2005GL024851](https://doi.org/10.1029/2005GL024851).
- B. D. Tapley, S. Bettadpur, M. Watkins, and C. Reigber. The gravity recovery and climate experiment: Mission overview and early results. *Geophysical Research Letters*, 31(9), 2004. doi:[10.1029/2004GL019779](https://doi.org/10.1029/2004GL019779).
- A. C. Thomas, J. T. Reager, J. S. Famiglietti, and M. Rodell. A GRACE-based water storage deficit approach for hydrological drought characterization. *Geophysical Research Letters*, 41(5):1537–1545, 2014. doi:[10.1002/2014GL059323](https://doi.org/10.1002/2014GL059323).
- M. J. Tourian. *Application of spaceborne geodetic sensors for hydrology*. 2013. doi:[10.18419/opus-3929](https://doi.org/10.18419/opus-3929).
- G. Tsakiris, A. Loukas, D. Pangalou, H. Vangelis, D. Tigkas, G. Rossi, A. Cancelliere, et al. Drought characterization. *Drought management guidelines technical annex*, pages 85–102, 2007.
- UN. Global water resources under increasing pressure from rapidly growing demands and climate change, according to new UN World Water Development Report. Technical report, 2012.
- J. Van Der Knijff, J. Younis, and A. De Roo. LISFLOOD: a GIS-based distributed model for river basin scale water balance and flood simulation. *International Journal of Geographical Information Science*, 24(2):189–212, 2010. doi:doi.org/10.1080/13658810802549154.
- A. Van Dijk. The Australian Water Resources Assessment System Technical Report 3. Landscape Model (version 0.5) Technical Description. 2010. doi:[10.4225/08/5852dd9bb578c](https://doi.org/10.4225/08/5852dd9bb578c).
- A. I. van Dijk, H. E. Beck, R. S. Crosbie, R. A. de Jeu, Y. Y. Liu, G. M. Podger, B. Timbal, and N. R. Viney. The Millennium Drought in southeast Australia (2001–2009): Natural and human causes and implications for water resources, ecosystems, economy, and society. *Water Resources Research*, 49(2):1040–1057, 2013. doi:[10.1002/wrcr.20123](https://doi.org/10.1002/wrcr.20123).
- M. Van Rooy. A rainfall anomaly index independent of time and space. *Notos*, 14(43):6, 1965.
- I. Velicogna and J. Wahr. Measurements of time-variable gravity show mass loss in Antarctica. *science*, 311(5768):1754–1756, 2006. doi:[10.1126/science.1123785](https://doi.org/10.1126/science.1123785).
- S. M. Vicente-Serrano, S. Beguería, and J. I. López-Moreno. A multiscalar drought index sensitive to global warming: the standardized precipitation evapotranspiration index. *Journal of climate*, 23(7):1696–1718, 2010. doi:[10.1175/2009JCLI2909.1](https://doi.org/10.1175/2009JCLI2909.1).

- R. R. von Frese, L. V. Potts, S. B. Wells, T. E. Leftwich, H. R. Kim, J. W. Kim, A. V. Golynsky, O. Hernandez, and L. R. Gaya-Piqué. GRACE gravity evidence for an impact basin in Wilkes Land, Antarctica. *Geochemistry, Geophysics, Geosystems*, 10(2), 2009. doi:[10.1029/2008GC002149](https://doi.org/10.1029/2008GC002149).
- Y. Wada, D. Wisser, and M. F. Bierkens. Global modeling of withdrawal, allocation and consumptive use of surface water and groundwater resources. *Earth System Dynamics*, 5(1): 15–40, 2014. doi:[10.5194/esd-5-15-2014](https://doi.org/10.5194/esd-5-15-2014), 2014.
- J. Wahr, M. Molenaar, and F. Bryan. Time variability of the Earth's gravity field: Hydrological and oceanic effects and their possible detection using GRACE. *Journal of Geophysical Research: Solid Earth*, 103(B12):30205–30229, 1998. doi:[10.1029/98JB02844](https://doi.org/10.1029/98JB02844).
- F. Wang, Y. Chen, Z. Li, G. Fang, Y. Li, X. Wang, X. Zhang, and P. M. Kayumba. Developing a long short-term memory (lstm)-based model for reconstructing terrestrial water storage variations from 1982 to 2016 in the tarim river basin, northwest china. *Remote Sensing*, 13(5):889, 2021. doi:[10.3390/rs13050889](https://doi.org/10.3390/rs13050889).
- J. Wang, D. Jiang, Y. Huang, and H. Wang. Drought analysis of the Haihe River Basin based on GRACE terrestrial water storage. *The Scientific World Journal*, 2014, 2014. doi:[10.1155/2014/578372](https://doi.org/10.1155/2014/578372).
- S. Wang and H. A. Russell. Forecasting snowmelt-induced flooding using GRACE satellite data: A case study for the Red River watershed. *Canadian Journal of Remote Sensing*, 42(3): 203–213, 2016. doi:[10.1080/07038992.2016.1171134](https://doi.org/10.1080/07038992.2016.1171134).
- M. M. Watkins and D.-N. Yuan. JPL Level-2 processing standards document for Level-2 product release 05. *GRACE Document*, pages 327–744, 2012.
- D. Wiese, D. Yuan, C. Boening, F. Landerer, and M. Watkins. Jpl grace and grace-fo mascon ocean, ice, and hydrology equivalent water height coastal resolution improvement (cri) filtered release 06 version 02, 2019. Last accessed: 1 February 2021.
- D. A. Wilhite. *Preparing for Drought: A Guidebook for Developing Countries*. 1992.
- D. A. Wilhite. *Drought as a natural hazard: concepts and definitions*. 2000.
- G. Willeke, J. Hosking, J. Wallis, and N. Guttman. The national drought atlas. *Institute for water resources report*, 94, 1994. doi:[10.1029/94EO00706](https://doi.org/10.1029/94EO00706).
- WMO. *Standardized Precipitation Index user guide.*, 2012.
- WMO. *WMO statement on the status of the global climate in 2012.*, 2013.
- B. Wouters, J. Bonin, D. Chambers, R. Riva, I. Sasgen, and J. Wahr. GRACE, time-varying gravity, Earth system dynamics and climate change. *Reports on Progress in Physics*, 77(11): 116801, 2014. doi:[10.1088/0034-4885/77/11/116801](https://doi.org/10.1088/0034-4885/77/11/116801).
- L. Xu, A. Samanta, M. H. Costa, S. Ganguly, R. R. Nemani, and R. B. Myneni. Widespread decline in greenness of Amazonian vegetation due to the 2010 drought. *Geophysical Research Letters*, 38(7), 2011. doi:[10.1029/2011GL046824](https://doi.org/10.1029/2011GL046824).
- H. Yi and L. Wen. Satellite gravity measurement monitoring terrestrial water storage change and drought in the continental United States. *Scientific reports*, 6:19909, 2016. doi:[10.1038/srep19909](https://doi.org/10.1038/srep19909).

- S. Z. Yirdaw, K. R. Snelgrove, and C. O. Agboma. GRACE satellite observations of terrestrial moisture changes for drought characterization in the Canadian Prairie. *Journal of Hydrology*, 356(1-2):84–92, 2008. doi:[10.1016/j.jhydrol.2008.04.004](https://doi.org/10.1016/j.jhydrol.2008.04.004).
- A. Zargar, R. Sadiq, B. Naser, and F. I. Khan. A review of drought indices. *Environmental Reviews*, 19(NA):333–349, 2011. doi:[10.1139/a11-013](https://doi.org/10.1139/a11-013).
- M. Zhao, I. Velicogna, and J. S. Kimball. A global gridded dataset of grace drought severity index for 2002–14: Comparison with PDSI and SPEI and a case study of the Australia millennium drought. *Journal of Hydrometeorology*, 18(8):2117–2129, 2017a. doi:[10.1175/JHM-D-16-0182.1](https://doi.org/10.1175/JHM-D-16-0182.1).
- M. Zhao, I. Velicogna, and J. S. Kimball. Satellite observations of regional drought severity in the continental United States using GRACE-based terrestrial water storage changes. *Journal of Climate*, 30(16):6297–6308, 2017b. doi:[10.1175/JCLI-D-16-0458.1](https://doi.org/10.1175/JCLI-D-16-0458.1).